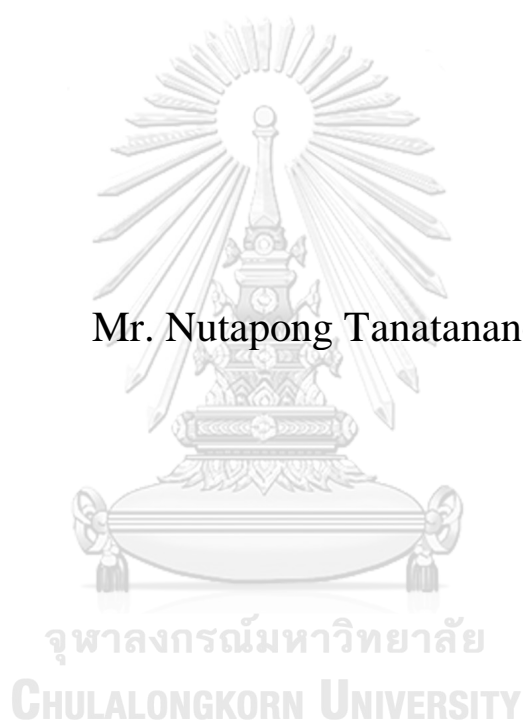


MOLECULAR DYNAMICS SIMULATION OF PHENOLIC  
COMPOUND ADSORPTION ON AMINE-  
FUNCTIONALIZED CARBON NANOTUBES

Mr. Nutapong Tanatananon



A Thesis Submitted in Partial Fulfillment of the Requirements  
for the Degree of Master of Science in Chemical Technology  
Department of Chemical Technology  
Faculty of Science  
Chulalongkorn University  
Academic Year 2019  
Copyright of Chulalongkorn University

การจำลองพลวัตเชิงโมเลกุลของการดูดซับสารประกอบฟีนอลิกบนท่อนาโนคาร์บอนดัดแปรด้วย  
หมู่ฟังก์ชันแอมีน



วิทยานิพนธ์นี้เป็นส่วนหนึ่งของการศึกษาตามหลักสูตรปริญญาวิทยาศาสตรมหาบัณฑิต  
สาขาวิชาเคมีเทคนิค ภาควิชาเคมีเทคนิค  
คณะวิทยาศาสตร์ จุฬาลงกรณ์มหาวิทยาลัย  
ปีการศึกษา 2562  
ลิขสิทธิ์ของจุฬาลงกรณ์มหาวิทยาลัย

Thesis Title	MOLECULAR DYNAMICS SIMULATION OF PHENOLIC COMPOUND ADSORPTION ON AMINE-FUNCTIONALIZED CARBON NANOTUBES
By	Mr. Nutapong Tanatananon
Field of Study	Chemical Technology
Thesis Advisor	Dr. Manaswee Suttipong

---

Accepted by the Faculty of Science, Chulalongkorn University in Partial  
Fulfillment of the Requirement for the Master of Science

..... Dean of the Faculty of Science  
(Professor Dr. POLKIT SANGVANICH)

#### THESIS COMMITTEE

..... Chairman  
(Associate Professor Dr. PRASERT  
REUBROYCHAROEN)

..... Thesis Advisor  
(Dr. Manaswee Suttipong)

..... Examiner  
(Associate Professor Dr. Patiparn Punyapalakul)

..... Examiner  
(Professor Dr. PORNPOTE PIUMSOMBOON)

..... External Examiner  
(Dr. Chompoonut Rungnim)



จุฬาลงกรณ์มหาวิทยาลัย  
CHULALONGKORN UNIVERSITY

ณัฐพงษ์ ธนธนานนท์ : การจำลองพลวัตเชิงโมเลกุลของการดูดซับสารประกอบฟีนอลิกบนท่อนาโนคาร์บอนดัดแปรด้วยหมู่ฟังก์ชันแอมีน. ( MOLECULAR DYNAMICS SIMULATION OF PHENOLIC COMPOUND ADSORPTION ON AMINE-FUNCTIONALIZED CARBON NANOTUBES) อ.ที่ปรึกษาหลัก : ดร.มนัสวี สุทธิพงษ์

อันตรกิริยาระหว่างสารประกอบฟีนอลิก (phenolic compound) ที่พบมากในใบชาเขียวได้แก่ เอพิกัลโลคาเทชิน -3-กัลเลต ((-)-epigallocatechin gallate, EGCG) และเอพิกัลโลคาเทชิน ((-)-epigallocatechin, EGC) กับหมู่ฟังก์ชันแอมีน (amine functional group) ที่ดัดแปรบนพื้นผิวท่อนาโนคาร์บอน (carbon nanotube, CNT) ถูกศึกษาด้วยการจำลองพลวัตเชิงโมเลกุล (molecular dynamics simulation) สารประกอบแอมีนที่สนใจคือ เอทิลีนไดแอมีน (ethylenediamine, EDA) ไตรเอทิลีนเตตราไมน (triethylenetetramine, TETA) และเมลามีน (melamine, MA) ผลการจำลองพลวัตเชิงโมเลกุลแสดงให้เห็นว่าโครงสร้างโมเลกุลของหมู่ฟังก์ชันแอมีนส่งผลต่อพฤติกรรมการแพร่และลักษณะการดูดซับของสารประกอบ EGCG และ EGC ท่อนาโนคาร์บอนที่ดัดแปรด้วยหมู่เอทิลีนไดแอมีน (EDA/CNT) สามารถดูดซับทั้ง EGCG และ EGC ได้ดีที่สุดและพบว่าสารประกอบฟีนอลิกทั้งสองชนิดใช้โครงสร้างวงแหวน 2 วง (bicyclic structure) เกิดอันตรกิริยากับหมู่ฟังก์ชันแอมีน EDA ที่มีสายโซ่สั้นจึงเคลื่อนที่ได้อย่างอิสระและระหว่างโมเลกุล EDA มีพื้นที่ว่างสำหรับการดูดซับของ EGCG และ EGC จึงส่งผลดีในการดูดซับ EGCG และ EGC ในทางกลับกันถ้าดัดแปรท่อนาโนคาร์บอนด้วย TETA หรือ MA พบว่าความสามารถในการดูดซับของ EGC และ EGCG ลดลง โดย TETA มีสายโซ่โมเลกุลยาวส่งผลให้เกิดการจับตัวกันเอง และ MA ที่โครงสร้างโมเลกุลมีวงแหวนเมื่อจัดเรียงตัวบนพื้นผิวท่อนาโนคาร์บอนทำให้เกิดการบดบังการดูดซับ นอกจากนี้เมื่อพิจารณาพฤติกรรมดูดซับของ EGCG และ EGC จากการศึกษาความหนาแน่นในแนวรัศมีและการคำนวณฟังก์ชันการกระจายเชิงรัศมี EGC ซึ่งมีขนาดโมเลกุลเล็กดูดซับบน EDA/CNT ได้ดีกว่า EGCG ที่มีขนาดโมเลกุลใหญ่ การจำลองพลวัตเชิงโมเลกุลทำให้เกิดความเข้าใจพื้นฐานในระดับโมเลกุลของการดูดซับระหว่างสารประกอบฟีนอลิกกับหมู่แอมีนบนท่อนาโนคาร์บอน ตลอดจนใช้เป็นแนวทางพัฒนาตัวดูดซับที่มีประสิทธิภาพต่อไป

จุฬาลงกรณ์มหาวิทยาลัย  
CHULALONGKORN UNIVERSITY

สาขาวิชา เคมีเทคนิค  
ปีการศึกษา 2562

ลายมือชื่อนิสิต .....  
ลายมือชื่อ อ.ที่ปรึกษาหลัก .....

# # 6071935123 : MAJOR CHEMICAL TECHNOLOGY

KEYWORD EGCG, EGC, Adsorption, Amine functional group

D:

Nutapong Tanatananon : MOLECULAR DYNAMICS SIMULATION OF PHENOLIC COMPOUND ADSORPTION ON AMINE-FUNCTIONALIZED CARBON NANOTUBES. Advisor: Dr. Manaswee Suttipong

The interactions between green tea phenolic compounds, including (-)-epigallocatechin gallate (EGCG) and (-)-epigallocatechin (EGC), and various amine groups functionalized on carbon nanotube (CNT) were studied by all-atom molecular dynamics (MD) simulations. The amine functional groups: ethylenediamine (EDA), triethylenetetramine (TETA), and melamine (MA) were considered in this study. Simulated results showed that amine molecular structure grafted on CNT surface affected diffusion and adsorption of EGCG and EGC. The EDA-functionalized CNT (EDA/CNT) provided a strong adsorption affinity to EGCG and EGC with their bicyclic segments located within the EDA layer. It is because the functionalized-EDA structure was well-defined and given empty site for adsorption. TETA showed dense packing with self-aggregation, resulting the difficulty in adsorption of EGCG and EGC. MA with aromatic amine structure oriented perpendicularly to the CNT axis, prevented the conjugating phenolic molecules to adsorb onto surface. In addition, the results obtained from radial density profiles and radial distribution functions suggested that the smaller EGC molecule adsorbed on the EDA/CNT greater than the larger EGCG molecule. The results obtained not only provide fundamental understanding on the adsorption process, but also complement experimental studies, and perhaps could design new sorbent materials for separation.

จุฬาลงกรณ์มหาวิทยาลัย  
CHULALONGKORN UNIVERSITY

Field of Study: Chemical Technology

Student's Signature

Academic 2019

Advisor's Signature

Year:

## ACKNOWLEDGEMENTS

I would like to express my sincere gratitude and appreciation to my advisor, Dr. Manaswee Sittipong. Without her persistent help this dissertation would not have been possible.

I am grateful to acknowledge Prof. Dr. Pornpote Piumsomboon, Assoc. Prof. Dr. Patiparn Punyapalakuland Dr. Chompoonut Rungnim for their time, patience and guidance throughout this dissertation.

I would like to sincerely thank National Electronics and Computer Technology Center (NECTEC) for computing facility. Particularly, I would like to appreciate Mr. Kajornsak Piyougkorn for his helpfulness in computational technique and simulated information.

Moreover, I would like to acknowledge the financial support by Science Achievement Scholarship of Thailand (SAST). I also thanks to all staffs of the Department of Chemical technology for their kind support.

Finally, I would like to supremely my deep gratitude to my family and friends for encouragement throughout this work.

Nutapong Tanatananon

# TABLE OF CONTENTS

	<b>Page</b>
.....	iii
ABSTRACT (THAI) .....	iii
.....	iv
ABSTRACT (ENGLISH) .....	iv
ACKNOWLEDGEMENTS .....	v
TABLE OF CONTENTS .....	vi
Chapter 1            Introduction .....	1
Chapter 2            Theory of Molecular Dynamics and Literature Reviews .....	3
2.1 Molecular dynamics (MD) simulation .....	3
2.1.1 Equation of motions .....	3
2.1.2 The Leap-frog algorithm .....	5
2.1.3 Cut-off distance and particle-mesh Ewald (PME) method .....	6
2.1.4 Periodic boundary conditions .....	6
2.1.5 Nose-Hoover thermostat.....	7
2.2 Literature reviews.....	8
2.2.1 Experimental studies .....	8
2.2.2 The computational studies.....	15
Chapter 3            Software and Methodology .....	16
3.1 Simulation software.....	16
3.1.1 MD Simulated software.....	16
3.1.2 High-performance computer connected software .....	16
3.1.3 Molecular building software .....	16
3.1.4 Molecular Dynamics visualized software .....	17
3.1.5 Computational calculated software .....	17
3.1.6 Text-publishing software.....	17

3.2 Methodology of MD simulations .....	18
3.2.1 Simulated systems .....	18
3.2.2 Force fields .....	19
3.2.3 Simulation algorithms .....	20
Chapter 4           Results and discussions .....	22
4.1 Structural properties of various amines functionalized on CNT .....	22
4.1.1 Simulation snapshots of amine functionalized CNT .....	22
4.1.2 Two-dimensional density plots .....	23
4.1.3 The radial density profiles of nitrogen atoms in amine functional groups	
24	
4.2 Surface diffusion and morphology of adsorbed EGCG and EGC on amine-	
functionalized CNT .....	26
4.2.1 Surface diffusion of adsorbed EGCG and EGC .....	26
4.2.1.1 Diffusion coefficient of EGCG or EGC on unfunctionalized CNT	
27	
4.2.1.2 Diffusion coefficient of adsorbed EGCG or EGC on amine-	
functionalized CNT .....	29
4.2.2 Adsorbed morphology of EGCG and EGC on amine-functionalized CNT	
32	
4.2.2.1 Simulation snapshots of ten EGCG or EGC molecules on amine-	
functionalized CNT .....	32
4.2.2.2 The radial density profile of EGCG or EGC .....	34
4.2.2.3 Radial distribution function (RDF).....	39
4.2.2.4 Binding energy ( <i>E<sub>binding</sub></i> ) .....	42
Chapter 5           Conclusions .....	46
Appendices.....	48
REFERENCES .....	65
VITA .....	69



## Chapter 1 Introduction

Phenolic compounds are natural antioxidants, found in plants, e.g. ginger, turmeric, chili, especially green tea [1]. The bioactive components in dry green tea leaves include 30% of catechin and 2-4.5 %wt. of caffeine. Catechin is a group of phenolic compounds, predominantly containing of (–)-epigallocatechin-3-gallate (EGCG), (–)-epigallocatechin (EGC), (–)-epicatechin-3-gallate (ECG), and (–)-epicatechin (EC) [2]. The green tea phenolic compounds, in particular EGCG, are powerful antioxidant, associated with the prevention of cancer, diabetes mellitus and cardiovascular diseases [3]. Separation and purification to phenolic components from green tea is an essential process. In the past decade, the separation and purification techniques of phenolic compounds have been developed into a method of adsorption onto porous materials since these materials are stable, good selectivity, large adsorption capacity, and structural diversity. In addition, the porous materials can be modified with functionalized molecules for enhanced adsorption properties [4, 5].

The adsorption of phenolic compounds on porous materials is governed by interaction between hydroxyl groups in phenolic compounds and solid sorbents, combining with weak intermolecular forces such as electrostatic interaction, hydrogen bonding, hydrophobic bonding, Van der Waals force, acid-base interactions, and/or  $\pi$ - $\pi$  stacking [6]. Previous experimental studies showed that amine or amino functional group can be used to modify porous materials to assist the adsorption of phenolic compounds. Type and distribution of amino groups on porous materials are factors in the adsorption processes [4-6]. However, the mechanism underlying the phenolic compound-induced adsorption of amine groups is not sufficiently well understood.

To date, molecular modelling has become an important tool to study structural and dynamic properties of substance adsorbed on solid sorbents, as well as to investigate material properties from an atomic point of view [7]. This work aims to study the surface diffusion and aggregation morphology of adsorbed phenolic compounds on amine-functionalized carbon nanotube (CNT) using molecular dynamics (MD) simulations, specifically to investigate the effect of amine molecular structure on

adsorption of phenolic compounds. The phenolic molecules considered were EGCG and EGC, shown in **Figure 1.1**. The amine molecules functionalized on CNT surface were ethylene diamine (EDA), triethylenetetramine (TETA), and melamine (MA), shown in **Figure 1.2**. The EDA is a short chain molecule with two nitrogen (N) atoms, while the TETA is a long chain amine functional group with four N atoms. The chemical structure of MA is composed of heteroaromatic of six N atoms. These N atoms are expected to interact with the hydroxyl groups in phenolic compounds via hydrogen bonding.

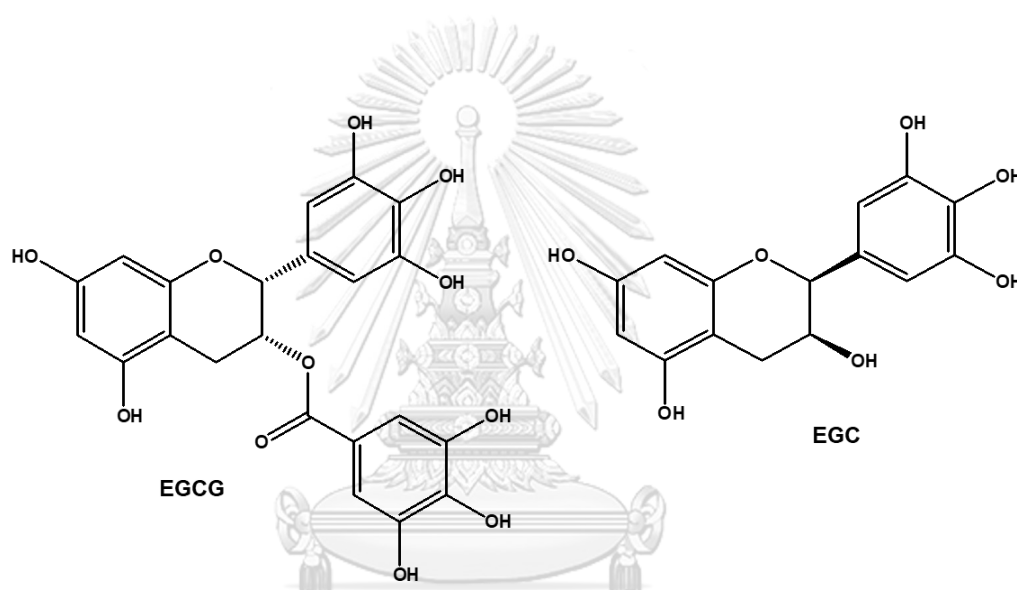


**Figure 1.1** Chemical structures of phenolic compounds, including epigallocatechin-3-gallate (EGCG) and epigallocatechin (EGC).

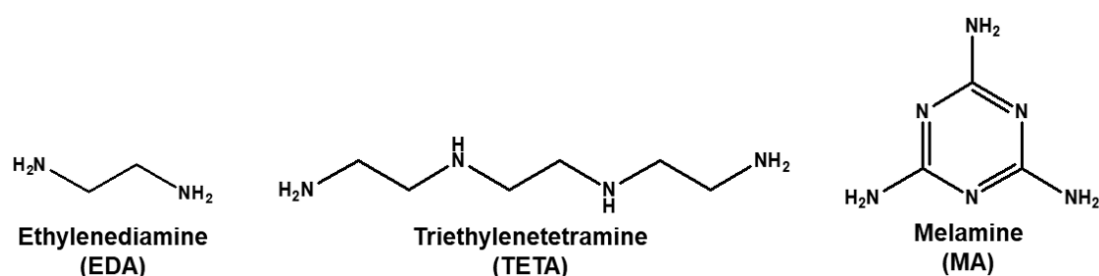


**Figure 1.2** Chemical structures amine functional groups, including ethylenediamine (EDA), triethylenetetramine (TETA) and melamine (MA).

## Chapter 2 Theory of Molecular Dynamics and Literature

### Reviews

This chapter presents the theoretical information of MD simulations and the literature reviews, which are explained in Sections 2.1 and 2.2, respectively.

#### 2.1 Molecular dynamics (MD) simulation

MD simulation is one of computational techniques that is extensively used as a common tool for investigating the structural properties and thermodynamics of molecular system [8]. Details of the background basic equation of motion in molecular dynamics, leap-frog algorithm to control the simulation time, the cut-off distance and particle-mesh Ewald (PME) method to simplify non-bonded interaction, periodic boundary conditions (PBC) and Nose-Hoover thermostat are described as follows in section 2.1.1, 2.1.2, 2.1.3, 2.1.4 and 2.1.5, respectively.

##### 2.1.1 Equation of motions

The basic concept in MD simulation is equation of motion, i.e. Newton's second law of motion, shown in **Equation (1)**, to solve all atomic motion of interesting system and provide trajectory results which are essential information to calculate micro and macroscopic properties.

$$\vec{F}_i = m_i \frac{d^2 \vec{r}_i}{dt^2} = m_i \frac{d\vec{v}_i}{dt}; i = 1, \dots, N \quad (1)$$

where  $\vec{r}_i$ ,  $\vec{v}_i$ ,  $m_i$ , and  $\vec{F}_i$  are the position, velocity, mass, and force of atom  $i$ , respectively.

To simulate the system, the input of initial configurations of interesting atoms are required. Such initial coordinates can be found from experiment literature or obtained from theoretical model. Initially, the configurations move randomly with velocities to Boltzmann distribution [8, 9]. The potential energy function ( $U$ ) is a driving force in Newton's equation to accelerate all interesting atoms [10], as shown in **Equation (2)**.

$$\vec{F}_i = -\nabla_{\vec{r}_i} U(\vec{r}_i); i = 1, \dots, N \quad (2)$$

The potential energy is a combining function of bonded and non-bonded interactions and can be written in **Equation (3)**. The bonded interaction energy includes bonds, angles and torsions of molecules, while the non-bonded interaction energies are van der Waals (vdW) and electrostatics interaction of pair atoms.

$$\begin{aligned}
 U(\vec{r}_i) = & \sum_{bonds} \frac{a_i}{2} (r_i - r_{i0})^2 + \sum_{angles} \frac{b_i}{2} (\theta_i - \theta_{i0})^2 \\
 & + \sum_{torsions} \frac{c_i}{2} [1 + \cos(n\omega_i - \gamma_i)] \\
 & + \sum_{atom\ pairs} 4\varepsilon_{ij} \left[ \left( \frac{\sigma_{ij}}{r_{ij}} \right)^{12} - \left( \frac{\sigma_{ij}}{r_{ij}} \right)^6 \right]^2 + \sum_{atom\ pairs} \frac{q_i q_j}{4\pi\varepsilon_0\varepsilon_r r_{ij}}
 \end{aligned} \quad (3)$$

The first term in potential energy function, the harmonic potential is modelled from covalent bonding in molecule, where  $r_i$  and  $r_{i0}$  are the bond length and the equilibrium bond length, respectively. The second term, the harmonic angle potential is corresponding bond angle formed between two bonding that sharing with one common atom. The bond angle vibration is represented by  $\theta_i$ , and  $\theta_{i0}$  (at equilibrium value). The third term, the proper dihedral properties is defined by the angle between two constrain planes in one molecule. The constrain planes consist of first plane (atoms 1-3) and the next plane (atoms 2-4) and can be rotated itself around same chemical bonding (atoms 2-3). The proper dihedral is the angle between two constrain planes when equal to zero corresponding to the cis configuration. The constant parameters of  $n$ ,  $\omega_i$  and  $\gamma_i$  are the periodic energy, current dihedral angle and the phase angle, respectively. In each molecule, the harmonic potential, the harmonic angle potential and the torsion angle potential are represented the properties of bonding interaction.  $a_i$ ,  $b_i$  and  $c_i$  are the force constants for the bonded, angle potentials and rotational energy barriers, respectively. The fourth term in potential energy function represents the repulsive and attractive forces from vdW and is described by the Lennard-Jones (LJ) potential.  $\varepsilon_{ij}$  is the minimum (well depth) of the

potential,  $\sigma_{ij}$  is the collision diameter, and  $r_{ij}$  is the distance between atoms  $i$  and  $j$ . Lorentz-Berthelot rules, as illustrated in **Equation (4)**, is applied to calculate  $\varepsilon_{ij}$  (geometric average) and  $\sigma_{ij}$  (arithmetic average).

$$\varepsilon_{ij} = \sqrt{\varepsilon_i \varepsilon_j} \text{ and } \sigma_{ij} = \frac{(\sigma_i + \sigma_j)}{2} \quad (4)$$

where  $\varepsilon_i$ ,  $\varepsilon_j$ ,  $\sigma_i$ , and  $\sigma_j$  are the well depths for the atoms  $i$  and  $j$  and the collision diameters for the atoms  $i$  and  $j$ , respectively. The fifth term is non-bonded interaction between two charge atomic particles (electrostatic interaction). There are various parameters:  $q_i$ ,  $q_j$ ,  $\varepsilon_0$ ,  $\varepsilon_r$  and  $r_{ij}$  represent charges of the atoms ( $i$  and  $j$ ), dielectric permittivity of vacuum, relative dielectric constant of medium and distance between atoms  $i$  and  $j$ , respectively.

### 2.1.2 The Leap-frog algorithm

The leap-frog algorithm was selected to integrate the equation of motion. The position, velocities and accelerations can be estimated from **Equations (5)** and **Equation (6)**, respectively.

$$\vec{r}_i(t + \Delta t) = \vec{r}_i(t) + \Delta t \vec{v}_i\left(t + \frac{1}{2} \Delta t\right) \quad (5)$$

$$\vec{v}_i\left(t + \frac{1}{2} \Delta t\right) = \vec{v}_i\left(t - \frac{1}{2} \Delta t\right) + \Delta t \vec{a}_i(t) \quad (6)$$

The velocities  $\vec{v}_i\left(t + \frac{1}{2} \Delta t\right)$  are calculated from the velocities at departure time  $\left(t - \frac{1}{2} \Delta t\right)$  and the accelerations at located time  $(t)$  (5). The positions of  $\vec{r}_i(t + \Delta t)$  can be analyzed from the positions at time  $(t)$  and the velocities  $\vec{v}_i\left(t + \frac{1}{2} \Delta t\right)$  from the previous step. Subsequently, the velocity at time  $(t)$  can be written as shown in **Equation (7)**.

$$\vec{v}_i(t) = \frac{1}{2} \left[ \vec{v}_i \left( t + \frac{1}{2} \Delta t \right) + \vec{v}_i \left( t - \frac{1}{2} \Delta t \right) \right] \quad (7)$$

The leap-frog algorithm provides the information of position coordinates over time step ( $\Delta t$ ). The optimization of time step ( $\Delta t$ ) is indispensable for simulating works. Using too small  $\Delta t$ , the simulation requires a lot of computational times for analysis data to equilibrium, while using too large  $\Delta t$ , the energy in equation of motion is rapidly increased that affects atomic movement significantly. In this dissertation,  $\Delta t$  of 2 fs was applied for all MD simulations.

### 2.1.3 Cut-off distance and particle-mesh Ewald (PME) method

The non-bonded interactions, including vdW and electrostatic interactions must be computed for each pair of atoms, causing high computational costs. Therefore, the cut-off distance is settled to separate the determination distance between pairs of atoms. The distance with greater values than cut-off distance is neglected. The vdW interaction can be approximated by cut-off distance method which more quickly calculated due to neglect all effect from distance atom that greater than the given cut-off distance [11]. However, the effect of electrostatic interaction decreases slowly with the distance and provides significant error. To handle this concern, Fourier-based particle-mesh Ewald (PME) method [12] was employed. The electrostatic interactions from short-range component calculates in real space, while the long-range component can be calculated using PME method.

### 2.1.4 Periodic boundary conditions

Periodic boundary conditions are commonly used in MD simulation as shown in the middle box in **Figure 2.1**. The periodic boundary conditions can be removed the boundary effects from system with finite size. After periodic boundary conditions are used, the motions of atoms in simulation box are in same direction as surrounding

atoms. For example, the simulation box as the center green box is generated from a large system in red box. Atoms A and B are moved out the simulation box but at the same time, another atoms A and B can be entered to the box from the opposite site. Hence, the physical boundaries condition of simulation box are not changed.

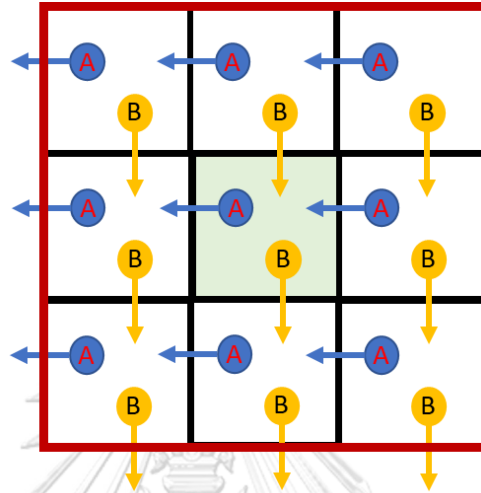


**Figure 2.1** Example of two-dimensional PBC. The simulation box is highlighted at the center.

### 2.1.5 Nose-Hoover thermostat

MD simulation is simulated under the canonical ensemble that condition is kept the number of atoms ( $N$ ), box volume ( $V$ ), and temperature ( $T$ ) to constant. Thermostat is required to control the temperature and avoid energy drifts caused by the accumulation of numerical errors. Especially, Nose-Hoover thermostat is an implement for efficiency relaxing to target temperature. The equation of motion is adapted accumulation  $\left(\frac{d^2\vec{r}_i}{dt^2}\right)$  when using Nose-Hoover thermostat, as shown in **Equation (8)**.

$$\frac{d^2\vec{r}_i}{dt^2} = \left(\frac{\vec{F}_i}{m_i}\right) - \left[\left(\frac{p\xi}{Q}\right)\frac{d\vec{r}_i}{dt}\right]; i = 1, \dots, N \quad (8)$$

where  $\xi$  is a dynamic quantity from particles accelerates when temperature ( $T$ ) approaches the desired value ( $T_0$ ).  $Q$  determines the relaxation energy from friction of molecules and the momentum of  $p\xi$  is derivatives from **Equation (9)**.

$$dp\xi/dt = (T - T_0) \quad (9)$$

The momentum of  $p\xi$  is an energy from departure temperature and evaluated from constant. It's considerable to influence of accumulation  $\left(\frac{d^2\bar{r}_i}{dt^2}\right)$  in simulated molecules.

## 2.2 Literature reviews

### 2.2.1 Experimental studies

Cotea and co-worker [13] studied the adsorption process of bioactive compounds separation in red wine using mesoporous molecular sieve silica or SBA-15. The structure of SBA-15 exhibited silicon-based adsorbed with silanol functional groups (Si-OH) and diverse pore size ranging from 3 to 30 nm. After the silica absorber had adsorbed red wine, the adsorption concentration of bioactive species was detected by HPLC, showed in **Figure 2.2**. The SBA-15 had been presented a selective property to adsorb phenolic compounds, especially quercetin (compound 18), compared with cis-resveratrol (compound 17), trans-resveratrol (compound 16), gallic acid (compound 1) and gentisic acid (compound 4). The phenolic compounds with similar structure to quercetin are preferable to adsorb on porous absorber. It is because of silanol functional groups.



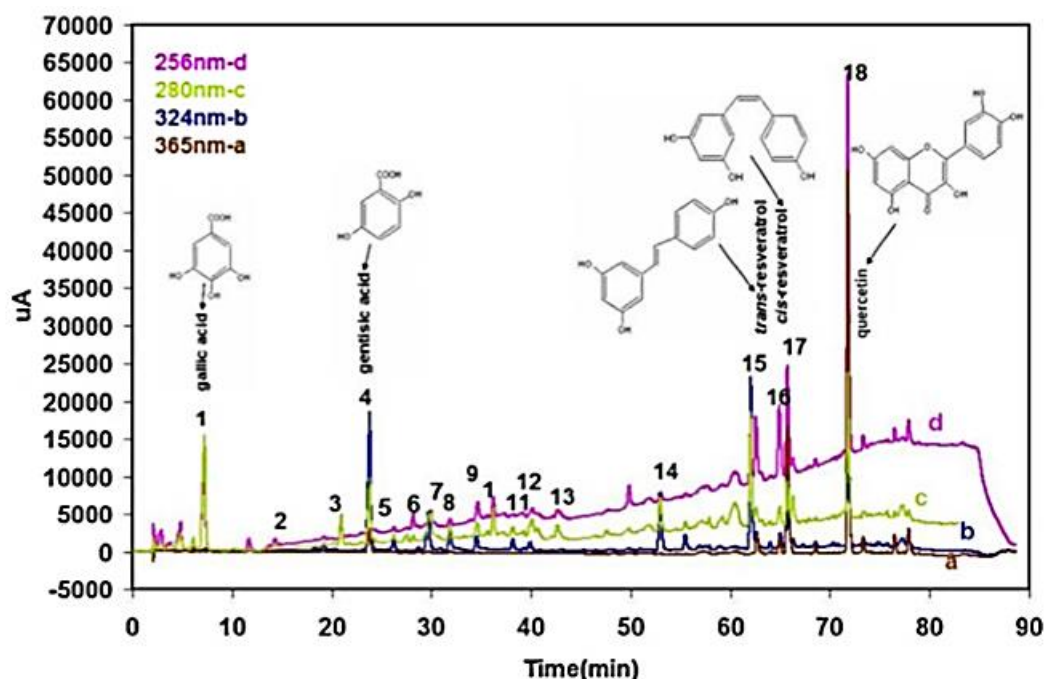


*Figure 2.2 Chromatograms of the extract of bioactive compounds from red wine which separated onto SBA-15 [13].*

In addition, the wastewater produced from olive mill manufacturing (OMW) process had found some phenolic compounds. The OMW is considerably destructive to the environment, but the phenolic compound can be recovered using mesoporous silica material. Yangui et al. [14] studied the extraction of phenolic compounds from OMW using mesoporous silica (SBA-15), commercial silica (P-10), and amine-modified mesoporous silica (TRI-SBA-15 and TRI-P-10). The amine modified material was synthesized from silica absorber (SBA-15 or P-10) by grafting method using 3-trimethoxysilylpropyl diethylenetriamine (TRI) and shown in **Figure 2.3**.

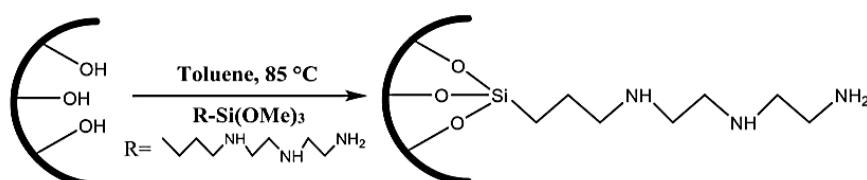


*Figure 2.3 The synthesis of amine-modified mesoporous silica [14].*

The constituents of wastewater were analyzed and contained two major products: hydroxytyrosol and tyrosol. Both of hydroxytyrosol and tyrosol are commercial phenolic compound with potential effect on human health such as antiatherogenic effect and anticancer effects, as like as EGCG and EGC [15]. In recovery process, the amine-modified mesoporous (TRI-SBA-15 and TRI-P-15) were showed better performance than non-modified mesoporous materials (SBA-15 and P-15) as shown in **Figure 2.4**.

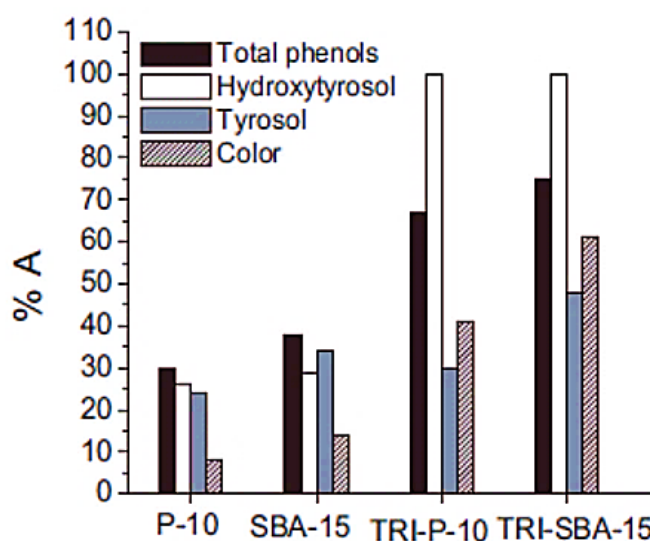


**Figure 2.4** The adsorption efficiencies (% A) of total phenols, hydroxytyrosol, tyrosol and dark color by using P-10, SBA-15, TRI-P-10 and TRI-SBA-15 [15].

จุฬาลงกรณ์มหาวิทยาลัย  
CHULALONGKORN UNIVERSITY

The hydroxytyrosol was higher hydroxyl group than tyrosol and showed more ability to adsorb on amine-modified mesoporous, compared to tyrosol. TRI-SBA-15 exhibited slightly higher adsorption efficiency of total phenolic compound than TRI-P-10. The adsorption mechanism was proposed in their paper. The hydrogen atom of the ammonium groups of amine compound interacted with the oxygen atom of hydroxyl group through hydrogen bonding interaction were illustrated in **Figure 2.5**.

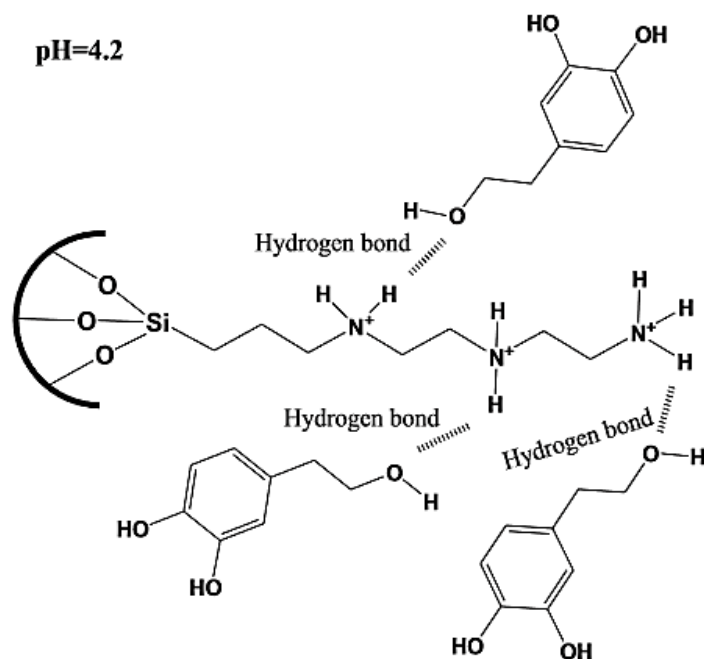


**Figure 2.5** The interaction mechanism between TRI-SBA-15 and hydroxytyrosol [15].

Likewise, the values from thermodynamic information of hydroxytyrosol adsorption showed enthalpy ( $\Delta_r H^\circ$ ) of TRI-SBA-15 was higher minus values than TRI-P-10 in the adsorption process, as showed in **Table 2.1**. The minus value of enthalpy means exothermic reaction to create hydrogen-bonding interaction. TRI-SBA-15 was preferable to adsorb hydroxytyrosol, compared to TRI-P-10. Briefly conclusion, this literature, the amine groups can be modified porous materials to increase the performance of phenolic compound adsorption.

**Table 2.1** Thermodynamic properties of hydroxytyrosol adsorption [15].

Temperature (K)	$K_c$ (L mg <sup>-1</sup> )	$\Delta_r H^\circ$ (KJ mol <sup>-1</sup> )	$\Delta_r S^\circ$ (KJ mol <sup>-1</sup> )	$\Delta_r G^\circ$ (KJ mol <sup>-1</sup> )
TRI-SBA-15				
293	51.409	-8.951	0.002	-9.597
313	39.876			-9.591
333	33.090			-9.688
TRI-P-10				
293	32.028	-7.682	0.003	-8.445
313	27.616			-8.635
333	21.878			-8.542

The phenolic compounds can be extracted from dried green tea. Zhao et al. [16] investigated the adsorption of tea phenolic compounds, using resin from crosslinked poly(N-vinyl-2-pyrrolidinone) or PVP-EGDMA-TAIC. The structure of PVP-DEGMA-TAIC are shown in **Figure 2.6**.

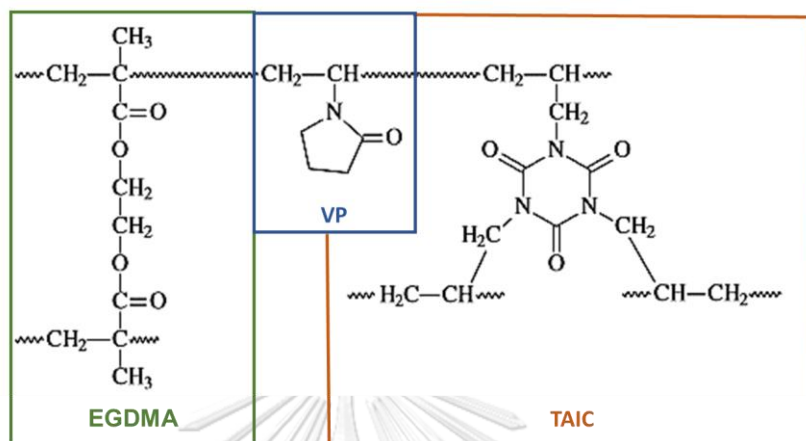


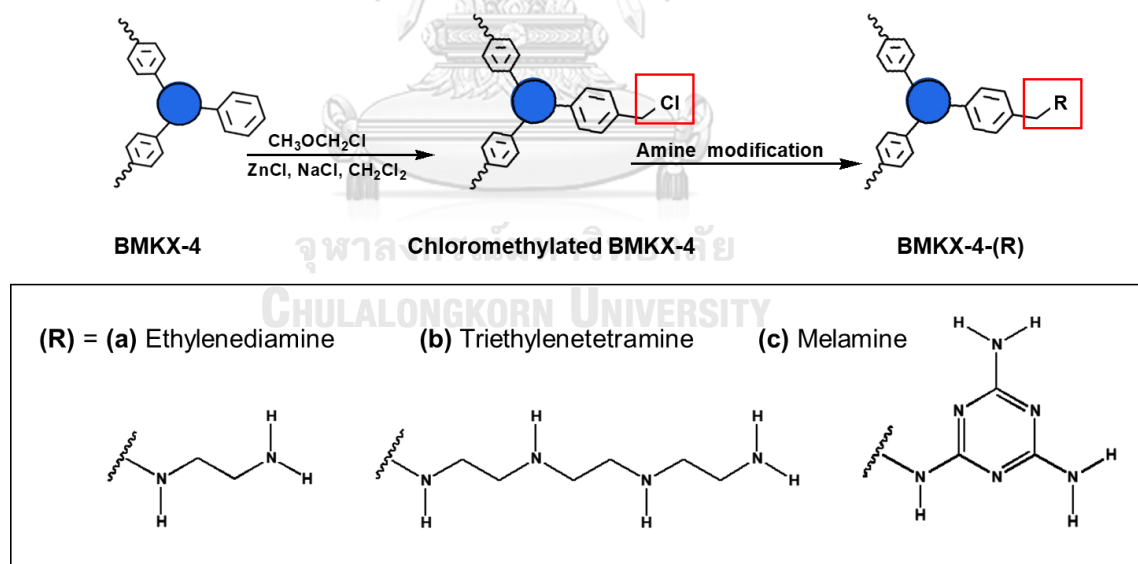
**Figure 2.6** Chemical structure of PVP-EGDMA-TAIC [16].

The crosslinked polymer was prepared from tri-block monomer copolymerization method which using N-vinyl-2-pyrrolidinone (VP), triallyl isocyanurate (TAIC), and ethylene glycol dimethacrylate (EGDMA) as monomers. The tea phenolic compound, especially EGCG, was adsorbed on PVP-DEGMA-TAIC with 92% removal, while caffeine was less adsorbed on PVP-DEGMA-TAIC with 4.3% removal as shown in **Table 2.2**. This polymer resin showed good selectivity of phenolic compound. Due to, the structure of PVP-DEGMA-TAIC, VP monomer has a major role about hydrophilicity and the amide group in the cyclic structure of VP may be easily formed hydrogen bonding interaction with EGCG molecule. On the other hand, TAIC and EGDMA were used to crosslinker molecule, providing moderate hydrophobic matrix with porous property. The absorber which contain a lot of porous and nitrogen atom in molecule can be provide a better performance of EGCG and prevent ability to adsorb caffeine.

**Table 2.2** The adsorption capacity of phenolic compound and caffeine [16].

Adsorbent	Phenolic compound		Caffeine	
	Capacity (mg/g)	Removal percentage (%)	Capacity (mg/g)	Removal percentage (%)
PVP-DEGMA-TAIC	92	92	0.84	4.3
ADS-5	20	23	5.4	33

The structural property of porous absorber, must be modified the surface with nitrogen functionalized molecules such as amine or amide, are essential factor to adsorb phenolic compound. Furthermore, Liu and co-worker [6] determined the effect of adsorption of tea phenolic compound, or EGCG, from different three amines functionalized on porous material. The mesoporous resin was synthesized by copolymerization with styrene and divinylbenzene to matrix material (BMKX-4). Then, three different amine molecules were grafted onto the resin to BMKX-4-(a), BMKX-4-(b), and BMKX-4-(c) as presented in **Figure 2.7**.

**Figure 2.7** The synthesis of three different amine modified BMKX-4 [6].

After synthesization, the surface characterization showed BMKX-4-(a) was homogeneous pores more than other material. BMKX-4-(b) had a greater number of amine groups than BMKX-4-(a) and BMKX-4-(c).

The trend of the adsorption capacity of EGCG was showed in **Figure 2.8**. The plot between adsorption capacity versus contact time showed the adsorption capacity of BMKX-4-(a) > BMKX-4-(b) = BMKX-4 > BMKX-4-(c). The adsorption capacity of porous modified with melamine, BMKX-4-(c), was steric hindrance structure. It was unfavorable to adsorb EGCG. From the results, Liu et al. explain that the polarity matching with amine functional groups was not dominant factor and geometrical matching and homogeneous pore also play an important role for distribution of EGCG onto porous material. The mechanical and chemical mechanisms were therefore essential factor in adsorption process.

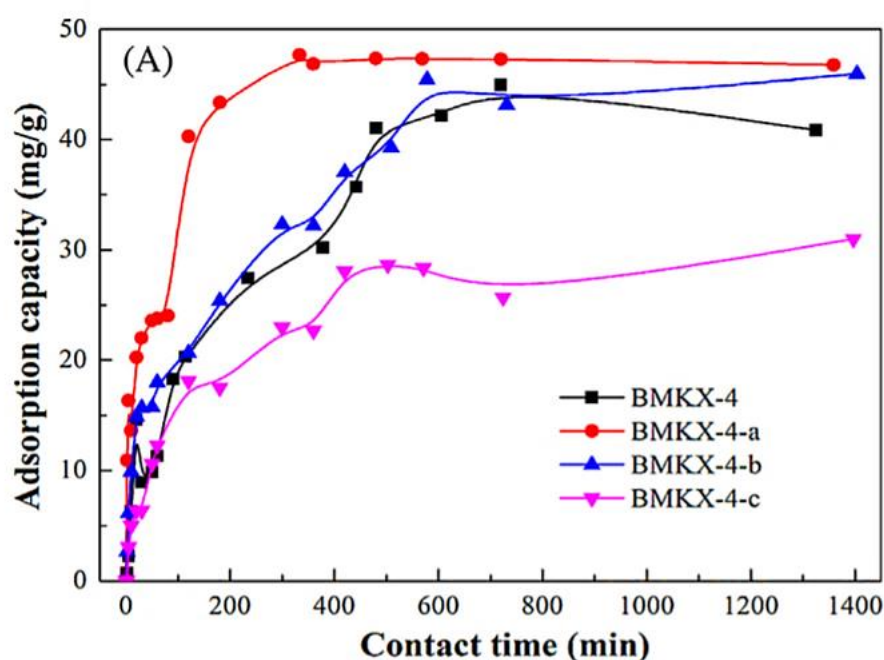


*Figure 2.8 Effect of contact time on adsorption of EGCG [6].*

For the considerate of mechanical and chemical adsorption of amine molecules affect to phenolic compound adsorption, the MD simulation is a computational technique to study the adsorption behaviour in atomic scale.

### 2.2.2 The computational studies

CNT is widely used in many applications as adsorbate material in molecular dynamic (MD) simulation because its rigid rod and hard to break the carbon-carbon bonding [17]. In addition, the surface of CNT can be added some functionalized molecules and then it can be enhanced properties of CNT [18, 19]. For example, Khare et al. [20] studied interfacial interaction of modified amido-amine functionalized nanotube (FCNT) which modified carbon nanotube by four amido-amine group. The FCNT were used for cross-linked reaction with epoxy nanocomposites and it can be enhanced the thermal properties of cross-linked nanocomposites. The simulated structure of amido-amine functionalized carbon nanotube was shown in **Figure 2.9**.

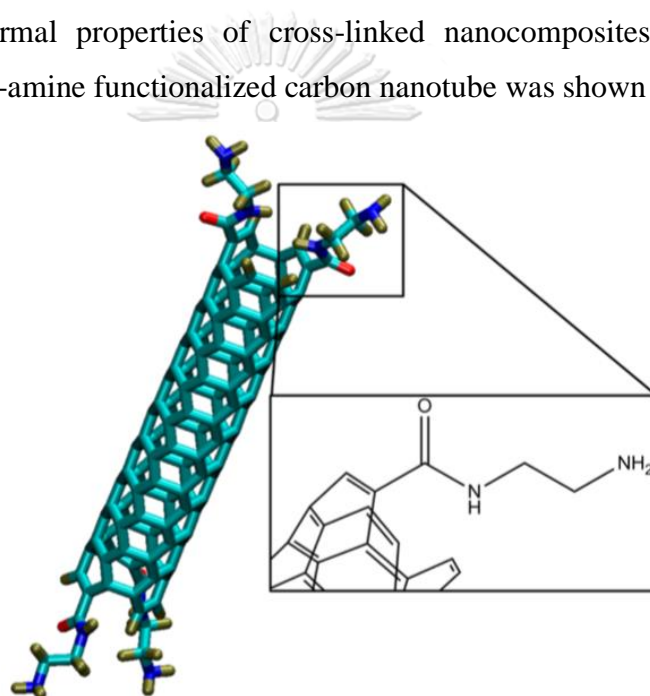


**Figure 2.9** Molecular model of functionalized CNTs [17].

*Color code: cyan for carbon atoms, red for oxygen atoms, blue for nitrogen atoms, and grey for hydrogen atoms.*

Khare and coworker simulated system of FCNT in water using LAMMPS package. All atoms in amido-amine molecules were applied the inter- and intra-molecular interaction with the general AMBER force field [21] and the partial charges on the atoms were determined using the AM1-BCC method [22]. In this dissertation, the simulations of various amine molecules were functionalized on surface of CNT.



## Chapter 3 Software and Methodology

This chapter presents simulation software and methodology that were used in this dissertation. Details of simulation software and methodology are explained in section 3.1 and 3.2, respectively.

### 3.1 Simulation software

#### 3.1.1 MD Simulated software

All systems in dissertation are investigated by GROMACS package, version 5.0.4 [23]. GROMACS is one fastest simulator software, most popular available using, and very flexible for various work. In this dissertation, GROMACS were installed via high performance computer (HPC) cluster “Hydrogen”, located at National Electronics and Computer Technology Centre (NECTEC).

#### 3.1.2 High-performance computer connected software

Two software: WinSCP and PuTTY, were considered to handle the simulated information between PC (or Notebook) and HPC. WinSCP is open source freeware for window which has function to manage files with remote computer. PuTTY is open source emulator which are available for Unix-like platforms. The function of PuTTY is used for support WinSCP function to network file transfer and directly commanded to compute result in HPC.

#### 3.1.3 Molecular building software

Material studio 2017 is a simple software for writing and modeling molecules on Windows. The information from molecular modeling can be suggested to MD simulation, for example, bond distance and atomic coordination.

ChemDraw Ultra 8.0 is a molecular editing software. Not only the software is easily edited the chemical structure, but also it can be approximately optimized structure and given some properties that are useful for MD simulation.



### 3.1.4 Molecular Dynamics visualized software

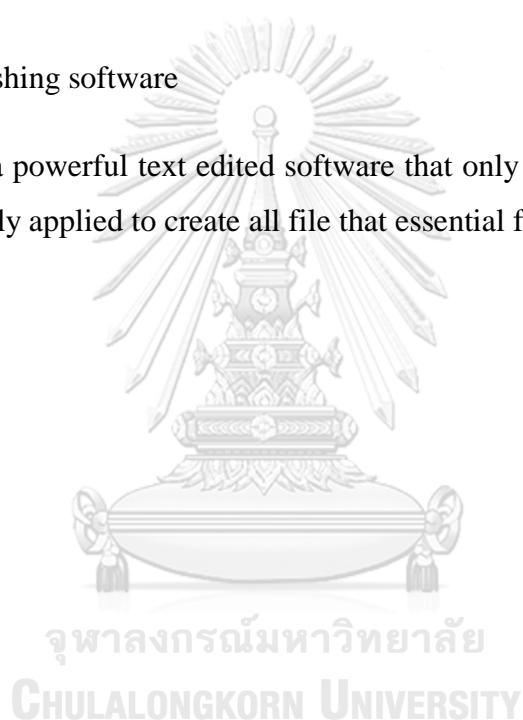
Visual Molecular Dynamics (VMD) is a commonly useful program in MD simulation for displaying, animating, and analyzing of interesting molecule.

### 3.1.5 Computational calculated software

In this dissertation, MATLAB R2018 was a computational calculating software for writing algorithm which appoints to analyze of some simulation results such as atomic density profiles.

### 3.1.6 Text-publishing software

EditPad Lite 7 is a powerful text edited software that only support on windows. This program is normally applied to create all file that essential for MD simulation.



## 3.2 Methodology of MD simulations

The detail of system compositions, force fields, and simulation algorithms of all simulation are briefly explained in Section 3.2.1, 3.2.2 and 3.2.3, respectively.

### 3.2.1 Simulated systems

The components of simulated system are shown in **Figure 3.1**. An example of simulated system: ten molecules of EGC adsorbed on EDA-functionalized CNT (EDA/CNT) in simulation box with size of  $9.6 \times 4.9 \times 9$  nm<sup>3</sup> was demonstrated in **Figure 3.2**.

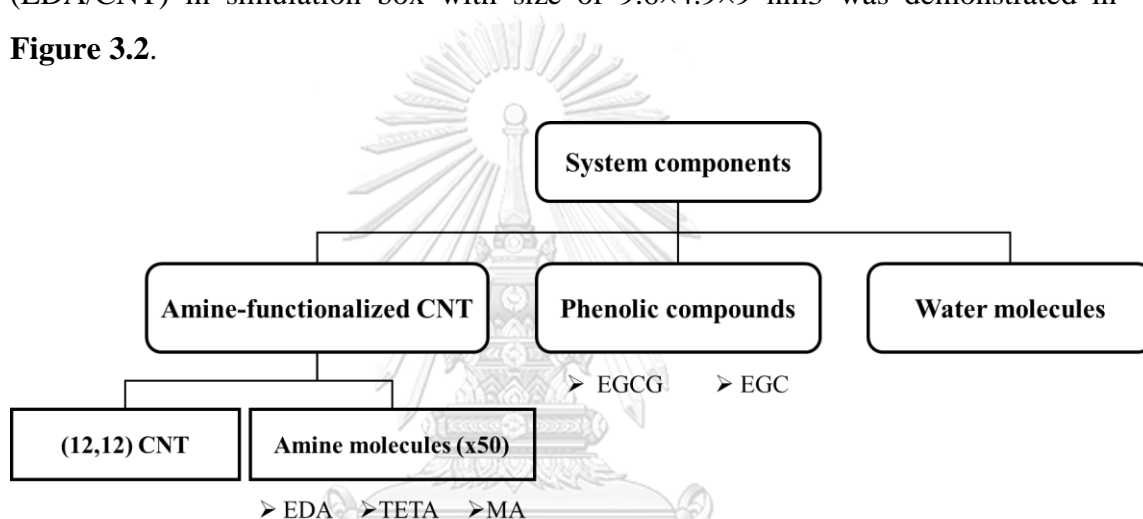


**Figure 3.1** The system components in this simulation work.

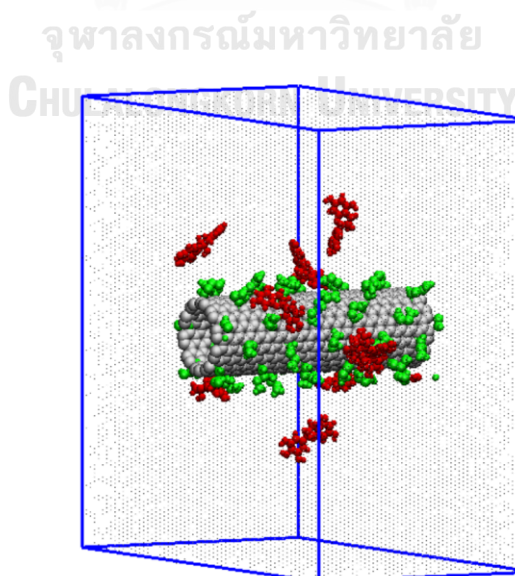


**Figure 3.2** Example of a simulated system. Color code: gray for CNT; green for grafted-EDA molecules; red for EGC compounds. Water molecules are transparent.

The amine-functionalized CNT was comprised of (12,12) CNT (Gray color) and amine molecules (Green color). CNT was maintained rigid at the center of the simulation box with fifty amine molecules, functionalized on the CNT surface. The cylindrical axis of the amine-functionalized CNT was aligned along the y direction of the simulation box. The phenolic compound, EGCG or EGC (Red color), were randomly located around the amine functionalized CNT. To study the diffusivity of adsorbed phenolic compound on amine-functionalized CNT, one molecule of EGCG (or EGC) were considered. The systems of ten molecules of EGCG or EGC were simulated to investigate the adsorption behavior. Finally, water molecules were added into the simulation box, reproducing bulk liquid water density at ambient conditions. While the positions of all atoms were changed overtime, the CNT was kept rigid.

### 3.2.2 Force fields

The force field is an essential simulation data to provide all parameters in bonded interaction and non-bonded interaction from potential energy. Therefore, the suitable selection of forcefield is important to provide reliable simulated information. In this dissertation, the carbon atoms within carbon nanotubes (CNT) was treated as a rigid molecule and showed the trajectory coordinate (x, y, z) of all carbon atom to constant. The matched model to simulate CNT was united-atom Lennard-Jones forcefield, which was proposed by Martin and Siepmann [24]. Three amine molecules (EDA, TETA and MA) and two phenolic compounds (EGCG and EGC) modelled using AMBER forcefield follow Hornak et al. [21]. In this model, AMBER force field was described as an appropriate forcefield to explain the biomolecule such as protein, peptide and so on [21, 25]. Water molecules were modelled using the transferable intermolecular potential with three points (TIP3P) model [26].

### 3.2.3 Simulation algorithms

Before initiating the MD simulation, the energy minimization was performed to relax the initial system. The relaxed conformation with low energy was obtained. Next, the system obtained was applied to simulate with GROMACS, version 5.0.7. The equation of motion for all atoms was integrated overtime by using the leap-frog algorithm. In addition, the time steps operated to simulated system were different variated dependent on type of graft amine: EDA or TETA was 0.002 ps and MA was 0.001 ps. The simulations were conducted within the canonical ensemble in which the number of particles (N), the box volume (V), and the temperature (T) were kept constant. The temperature was carried out at 300 K by using the Nose-Hoover thermostat. The van der Waals interactions were treated to non-bonded interaction when the distant of pair atoms below than cut-off distant at 9 Å. The particle mesh Ewald (PME) method was maintained to long-range electrostatic interactions. The trajectory coordinate and velocity of simulation atoms were saved every 1000 steps and the simulated times, in this dissertation, were showed in **Table 3.1**. In this work, the equilibrium condition was determined from the result of atomic density that not significantly changed interval the last 5 ns of simulation times. The simulated systems employed in this study and the corresponding simulation time are summarized in **Table 3.1**

**Table 3.1** Simulated systems employed in this study and the corresponding simulation time.

Amines-functionalized CNT	Phenolic compounds		Simulation times (ns)
	EGCG (molecule)	EGC (molecule)	
EDA/CNT	-	-	20
	1	-	20
	-	1	20
	10	-	60
	-	10	60
TETA/CNT	-	-	20
	1	-	20
	-	1	20
	10	-	60
	-	10	60
MA/CNT	-	-	20
	1	-	20
	-	1	20
	10	-	35
	-	10	40

## Chapter 4 Results and discussions

This chapter presents the results of structural properties of various amines functionalized on CNT, surface diffusion, and morphology of adsorbed EGCG and EGC on amine-functionalized CNT.

### 4.1 Structural properties of various amines functionalized on CNT

#### 4.1.1 Simulation snapshots of amine functionalized CNT

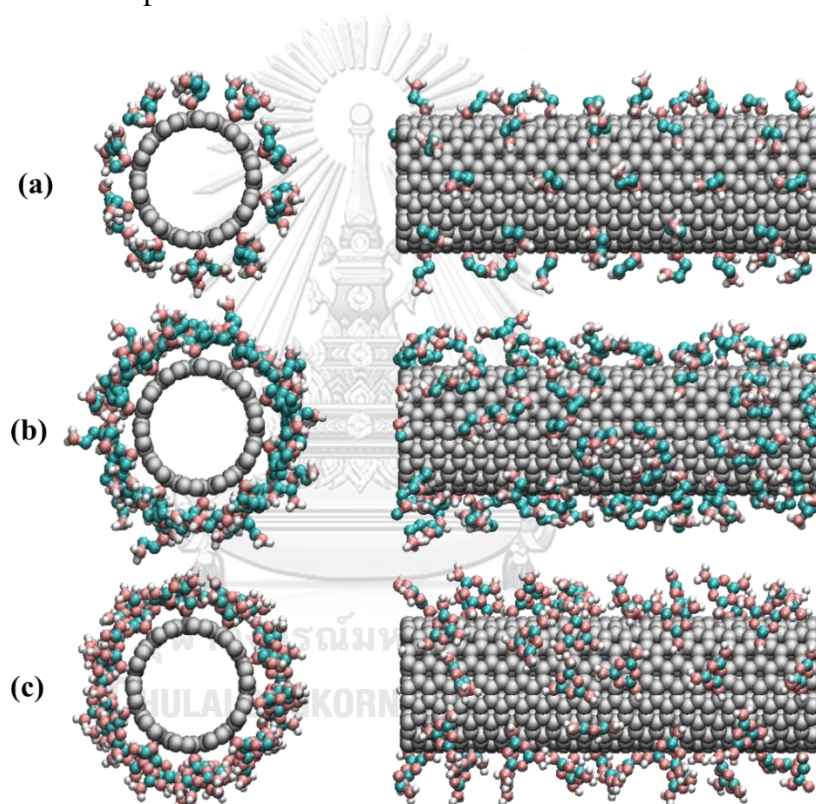


**Figure 4.1** Front (left panels) and side (right panels) views of representative simulation snapshots of (a) EDA functionalized on CNT (EDA/CNT), (b) TETA functionalized on CNT (TETA/CNT) and (c) MA functionalized on CNT (MA/CNT). Water molecules are not shown for clarity. Color code: cyan for carbon groups; white for hydrogen atoms; pink for nitrogen atoms; grey for carbon atoms in CNT.

**Figure 4.1** shows front (left) and side (right) views of equilibrium simulation snapshots for various amine molecules functionalized on CNT surface, including EDA (top panel), TETA (middle panel) and MA (bottom panel). The snapshots reveal

that the EDA molecules are located around the CNT with well-defined structure. It is noticed that the TETA and MA molecules pack densely around the carbon nanotube. Unexpectedly, TETA molecules with a long hydrocarbon preferentially located near the CNT surface, resulting dense packing aggregate structure. The simulation also suggests dense packing of MA aggregates due to a rigid heterocyclic in the MA molecules.

#### 4.1.2 Two-dimensional density plots

The two-dimensional contour plot in X and Z directions was calculated to further explain the simulation snapshot. The results are reported in **Figure 4.2**. The amine density is showed in different colors: low density is blue, which high density is red. It indicates that all amines, which are functionalized on the CNT, i.e., EDA/CNT, TETA/CNT, and MA/CNT, yield a monolayer. The short chain EDA molecules show the lowest packing density, compared to TETA and MA because the TETA and the MA contain long chain structure and heteroaromatic group, respectively.

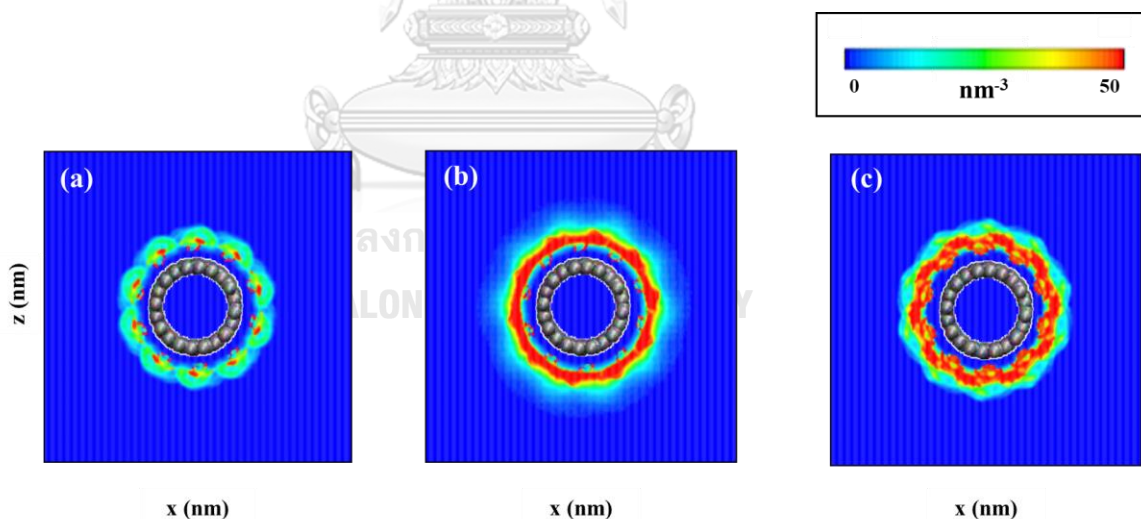


**Figure 4.2** Two-dimensional plots for the probability density of (a) EDA/CNT, (b) TETA/CNT and (c) MA/CNT.

#### 4.1.3 The radial density profiles of nitrogen atoms in amine functional groups

The radial density profile was calculated from atomic density in radial direction from surface of CNT. The structural observations are quantified by calculating density distributions of nitrogen atoms in EDA, TETA, and MA relative to the CNT surface. These results are reported in **Figure 4.3**. Top to bottom panels are obtained for EDA, TETA, and MA, respectively. Note that there are two, four, and six nitrogen atoms, in EDA, TETA, and MA molecules, respectively. The EDA contains N1 (black) and N2 (red). TETA comprises N1 (black), N2 (red), N3 (blue) and N4 (pink). MA is consisted of N1 (black), N5 (red), and N6 (blue) which are the nitrogen atoms around the heteroaromatic group, and N2, N3 and N4 (green) which are the nitrogen atoms within the heteroaromatic part.

The density profiles show that the nitrogen atom N1 for all amine groups is positioned close to the substrate as expected, yielding a shoulder at  $\sim 1.5$  Å and a peak at  $2.2$  Å. The nitrogen atom N2 of EDA extend to water with the density peak of high intensity at  $4$  Å. Unexpectedly, TETA with the nitrogen atoms N3 and N4 remain in the same position of N2, manifesting peaks at  $\sim 4$  Å. It is because hydrophobic repulsion between the non-ionic long chain of TETA and water [27]. Accordingly, it is observed self-aggregation of TETA, as shown in **Figure 4.3 (b)**. When the CNT is functionalized with MA, peaks at  $3.5$  Å and  $4.5$  Å in the density profiles are due to the nitrogen heteroatoms and the nitrogen atoms N5 and N6 next to the aromatic, respectively, corresponding to steric the hindrance structure of MA [6].



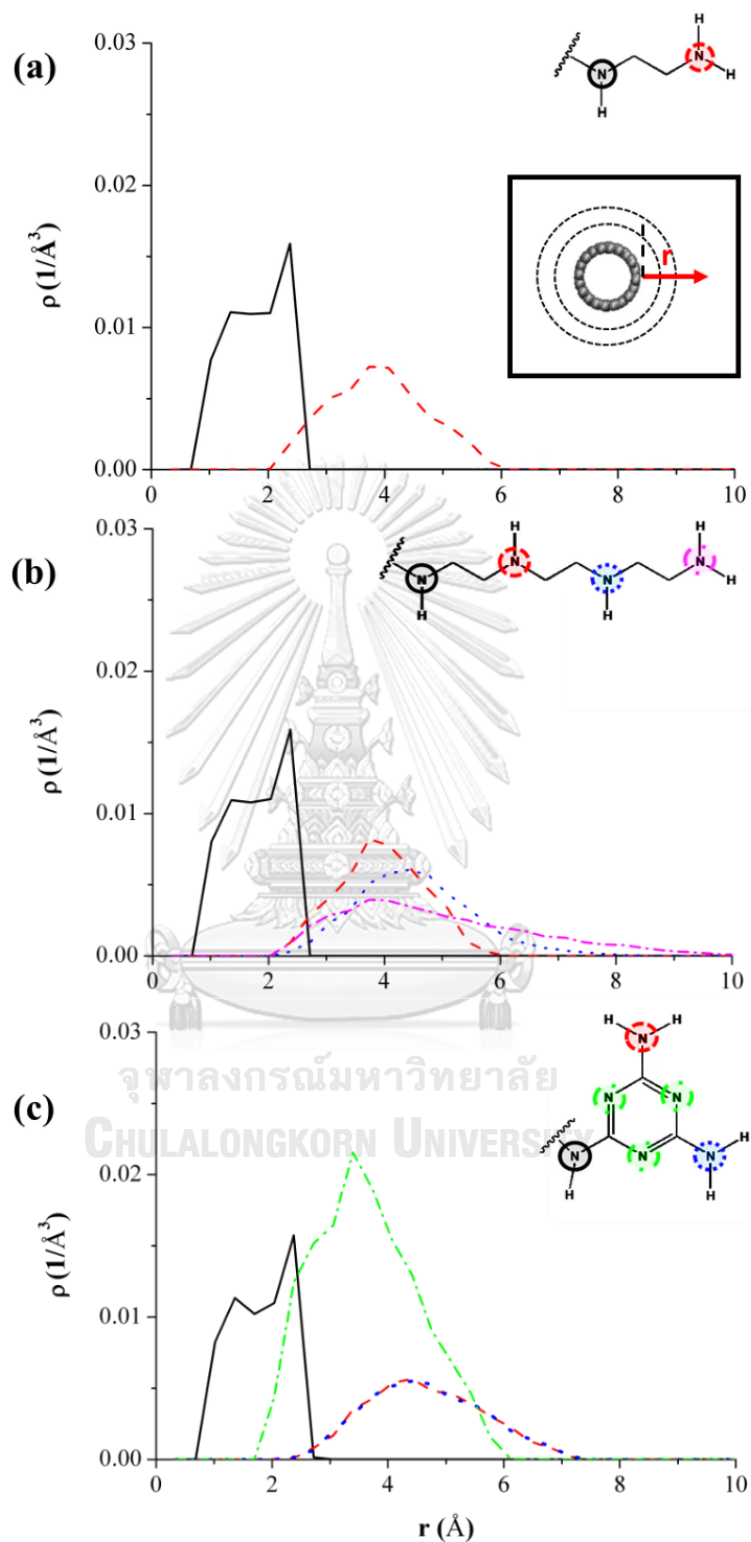


**Figure 4.3** Atomic density profiles of nitrogen atoms in functionalized (a) EDA, (b) TETA, and (c) MA relative to the CNT.  $r$  is measured radially from the nanotube surface

## 4.2 Surface diffusion and morphology of adsorbed EGCG and EGC on amine-functionalized CNT

### 4.2.1 Surface diffusion of adsorbed EGCG and EGC

The surface diffusion was investigated from the systems of one EGCG and EGC adsorbed on the formation later of pure CNT or amine functionalized on CNT. The results of surface diffusion on pure CNT and amine functionalized on CNT are showed in sections 4.2.1.1 and 4.2.1.2, respectively.

The surface diffusion is a rate of diffusion of active molecular dispersion. Higher diffusivity means that one respected substance faster diffuses to another region. In this dissertation, the surface diffusivity of EGC and EGCG adsorbed on amine-modified CNT, was investigated by diffusion coefficient (D) [28]. The diffusion coefficient is a physical constant of mass diffusing in time, following **Equation (10)**.

$$D = \frac{1}{6} \lim_{t \rightarrow \infty} \frac{d(MSD)}{dt} \quad (10)$$

where MSD is mean-square displacement. MSD is a function to average distance square of interesting particles in a period of times [29] as shown **Equation (11)**

$$MSD \equiv \langle (x - x_0)^2 \rangle = \frac{1}{N} \sum_{n=1}^N (x_n(t) - x_n(0))^2 \quad (11)$$

where  $x$  = The average position for all particle

$x_0$  = The reference position for all particle

$x_n(t)$  = The anytime position of each particle

$x_n(0)$  = The reference position of each particle

$n$  = Number of determine particle to be averaged

$N$  = Total particles to be averaged

#### 4.2.1.1 Diffusion coefficient of EGCG or EGC on unfunctionalized CNT

The diffusion coefficient between EGCG or EGC on functionalized CNT are investigated by MD simulation. The representation simulation snapshots for EGCG and EGC at (a) 2 ns, (b) 5 ns, and (c) 8 ns, are shown in **Figure 4.4** Front views (Top) and side view (bottom) of representation simulation snapshots of EGCG on the surface of CNT at (a) 2 ns, (b) 5 ns and (c) 8 ns. and **Figure 4.5** Front views (Top) and side view (bottom) of representation simulation snapshots of EGC on the surface of CNT at (a) 2 ns, (b) 5 ns and (c) 8 ns., respectively. The simulation snapshots show that there is no adsorption of either EGCG or EGC molecule on the CNT surface. The EGCG and EGC moves around the CNT. The movement of EGCG and EGC was investigated by MSD, plotted versus time, as shown in **Figure 4.6**. The MSD of EGCG and EGC increases with time. It is found that the MSD of EGCG is higher than that of EGC. **Table 4.1** shows high diffusion coefficient between EGCG or EGC and unfunctionalized CNT as equal to  $3.197$  and  $1.780 \times 10^{-5}$   $\text{cm}^2/\text{s}$ , respectively. These are related to the kinetic model of Ziaedini A. and coworker [30], who studied the extraction of antioxidants and caffeine.

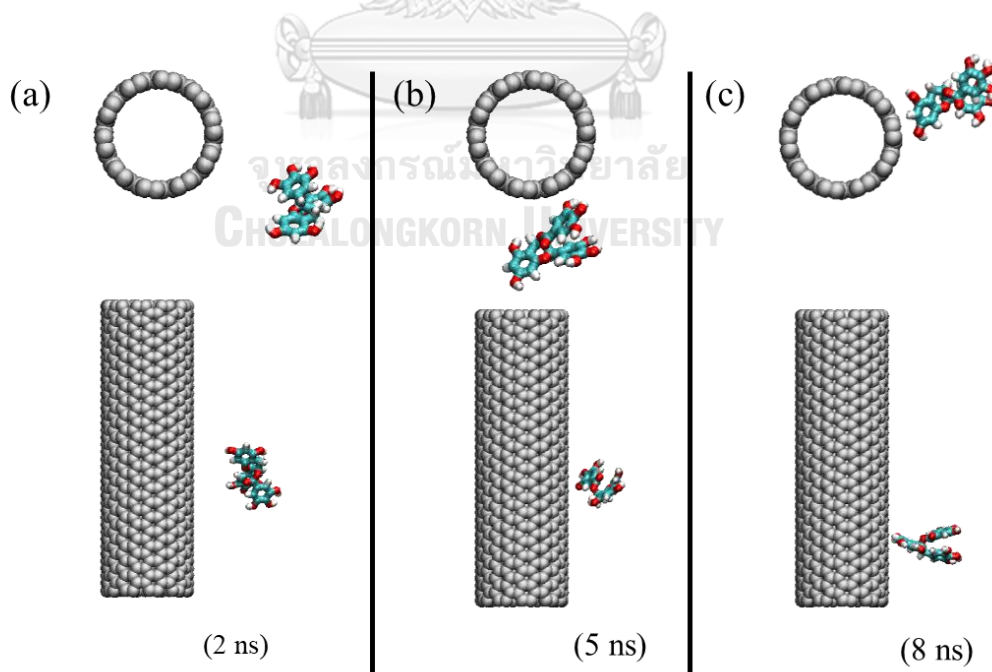


**Figure 4.4** Front views (Top) and side view (bottom) of representation simulation snapshots of EGCG on the surface of CNT at (a) 2 ns, (b) 5 ns and (c) 8 ns.

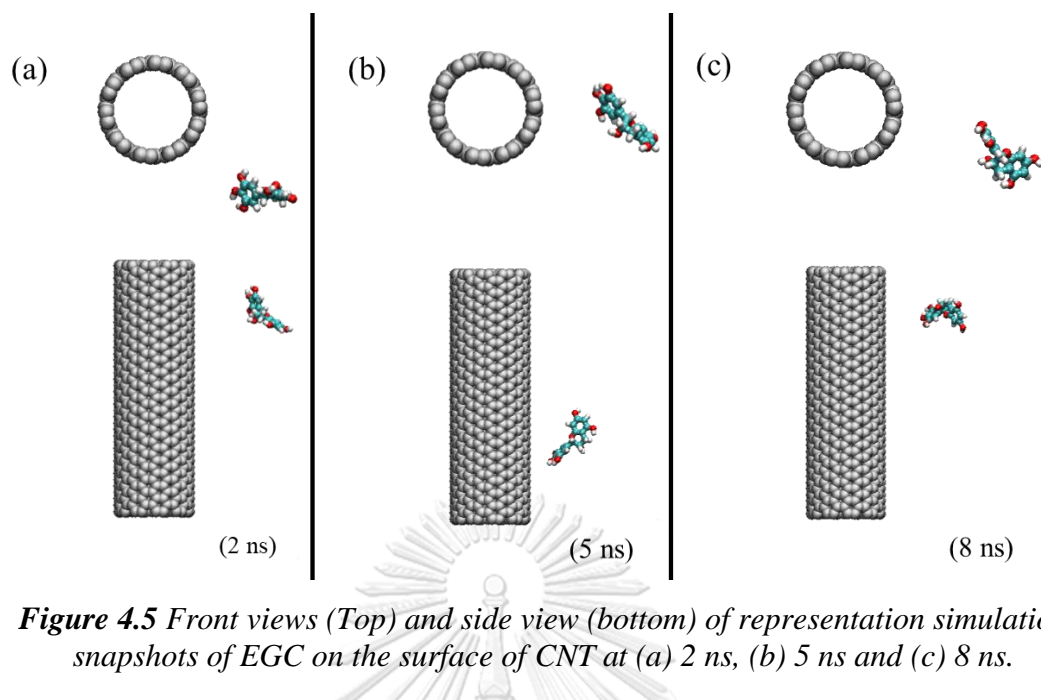


**Figure 4.5** Front views (Top) and side view (bottom) of representation simulation snapshots of EGC on the surface of CNT at (a) 2 ns, (b) 5 ns and (c) 8 ns.

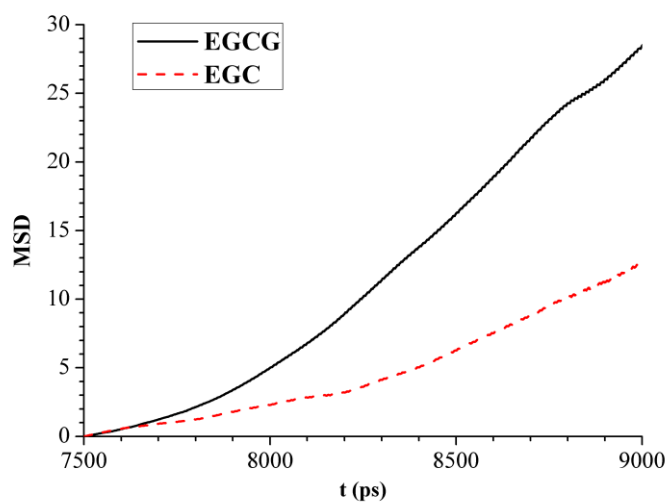


**Figure 4.6** Analysis of mean square displacement (MSD) versus time (t) from phenolic compound in system of CNT in water solution. The black-solid and red-dashed represent the results obtained from EGCG and EGC, respectively

**Table 4.1** Calculated diffusion coefficient (D) of EGCG and EGC on CNT.

	$D_{EGCG}$ ( $10^{-5}$ cm <sup>2</sup> /s)	$D_{EGC}$ ( $10^{-5}$ cm <sup>2</sup> /s)
<b>CNT</b>	3.197	1.780

#### 4.2.1.2 Diffusion coefficient of adsorbed EGCG or EGC on amine-functionalized CNT

The simulation snapshots of adsorbed EGCG or EGC on amine-functionalized CNT are shown in **Figure 4.7**. The EGCG molecule and the EGC molecule is adsorbed on three amine layers, EDA/CNT, TETA/CNT, and MA/CNT. It is noticed that the cyclic ring of EGCG molecule tends to position into the solution because large molecular structure of EGCG cannot penetrate into the layer of these amines.

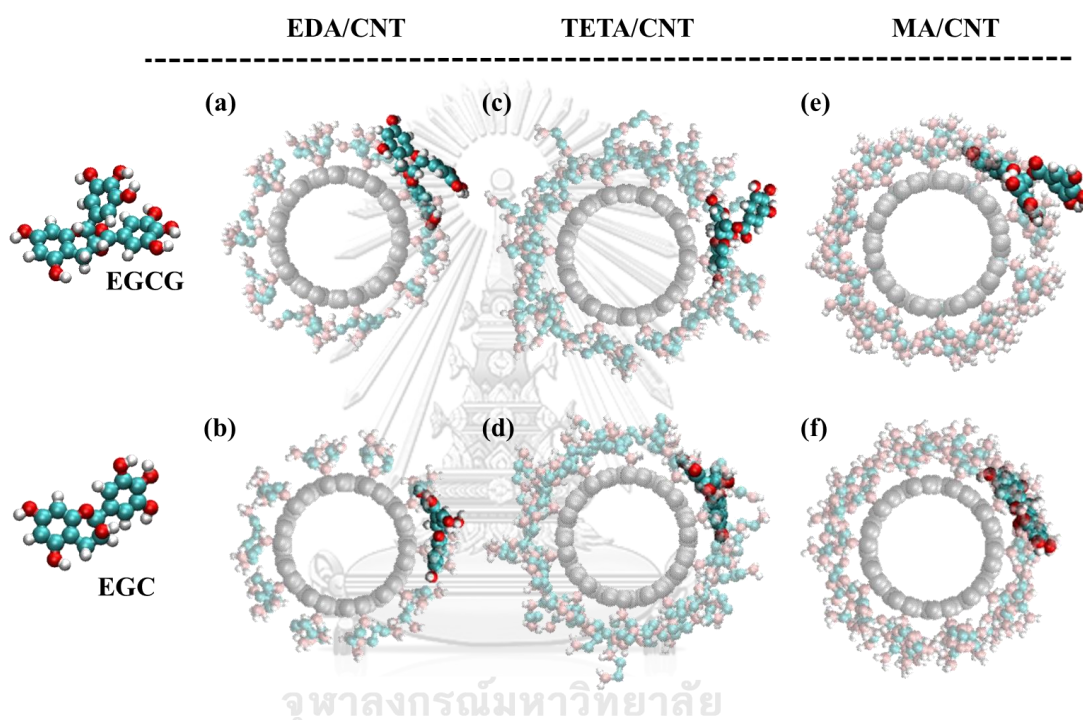


**Figure 4.7** Front views of representation simulation snapshots of EGCG (top panel) and EGC (bottom panel) on the surface of (a, b) EDA/CNT, (c, d) TETA/CNT and (e, f) MA/CNT. The molecules of EGCG and EGC are highlighted and the amine groups functionalized CNT are transparent. Color code: cyan for carbon groups; white for hydrogen atoms; pink for nitrogen atoms; red for oxygen atoms; grey for carbon atoms in CNT.

**Figure 4.8** shows the plots between MSD and time obtained for one molecule of EGCG and one molecule of EGC adsorbed on various amine-functionalized CNT during the simulation time of 7.5 – 8.5 ns. The MSD values of adsorbed EGCG and EGC on EDA/CNT are lower than those obtained on TETA/CNT and MA/CNT. The high value of MSD is related to the fast movement molecule on the surface, and

perhaps desorption of adsorbed species. Evidently, the adsorbed EGC on MA/CNT shows the highest MSD since during the course of simulation. From the slope of the linear dependence of the MSD plot, the diffusion coefficient can be obtained. The linear slope from the MSD plot was calculated in range of 8000 ps to 8500 ps for adsorbed EGCG, and range of 7500 ps to 8000 ps for adsorbed EGC. The diffusion coefficients are summarized to



**Table 4.2**, in units of  $10^{-5} \text{ cm}^2/\text{s}$ .

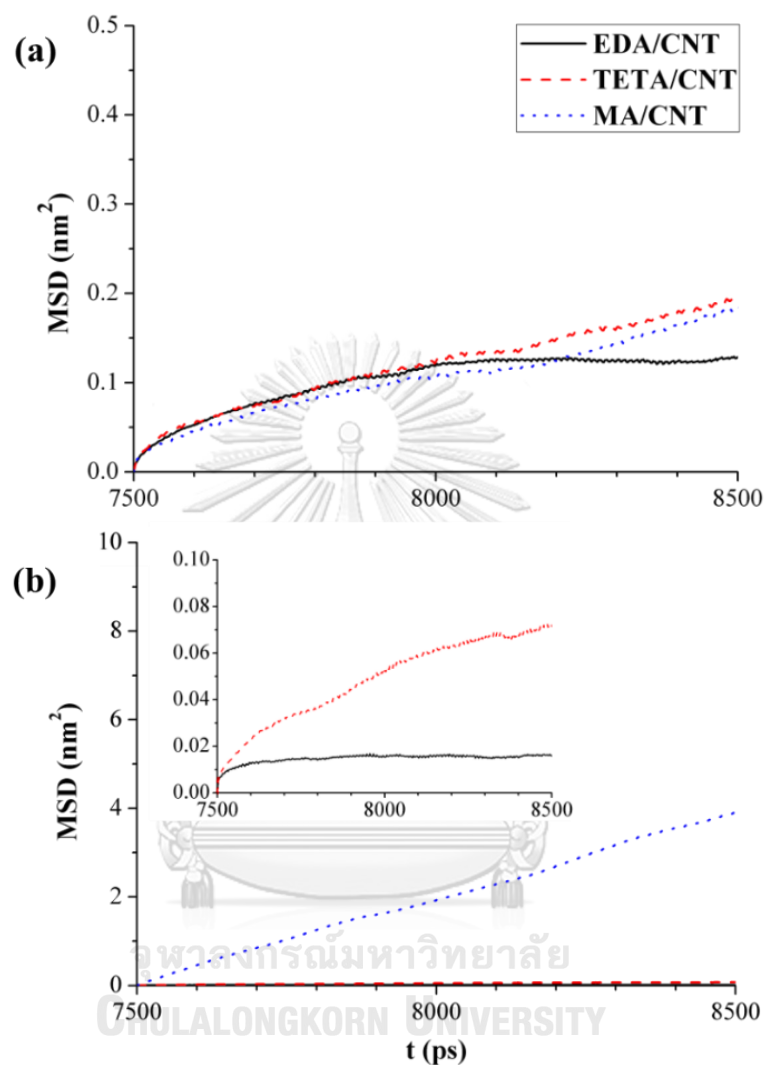


**Figure 4.8** Analysis of mean square displacement (MSD) versus time ( $t$ ) from adsorbed phenolic compound: (a) EGCG, (b) EGC and amine functionalized on CNT surface. The black-solid, red-dashed and blue dot lines represent the results obtained from EDA/CNT, TETA/CNT and MA/CNT, respectively

**Table 4.2** Calculated diffusion coefficient ( $D$ ) of EGCG and EGC on amine-functionalized CNT.

$D$ ( $10^{-5} \text{ cm}^2/\text{s}$ )	Amine-functionalized CNT		
	EDA/CNT	TETA/CNT	MA/CNT
EGCG	0.00425	0.03470	0.03750
EGC	0.00090	0.01150	0.18300

**Table 4.2** shows the lowest diffusion coefficient between EDA/CNT and EGCG (or EGC) as equal to 0.00425 and  $0.0009 \times 10^{-5} \text{ cm}^2/\text{s}$ , respectively. The diffusivity of adsorbed EGCG or EGC on EDA/CNT is lower than those obtained on TETA/CNT and MA/CNT, respectively ( $D_{\text{EDA/CNT}} < D_{\text{TETA/CNT}} < D_{\text{MA/CNT}}$ ), indicating favorable adsorption of EGCG and EGC on the EDA/CNT. It is due to the short chain of EDA molecule, which can provide adsorption site. The diffusion coefficient of EGC is found to be lower than EGCG. It is because EGCG moves around the amine-functionalized nanotube, induced by the interactions between the cyclic ring of EGCG molecule and the functionalized amine. For the system of MA/CNT, the EGC desorbs from the surface (**Figure 4**). The diffusivity of EGC is thus greater EGCG. It should be noted that the MA with rigid aromatic segment does not provide a good performance for EGC adsorption.



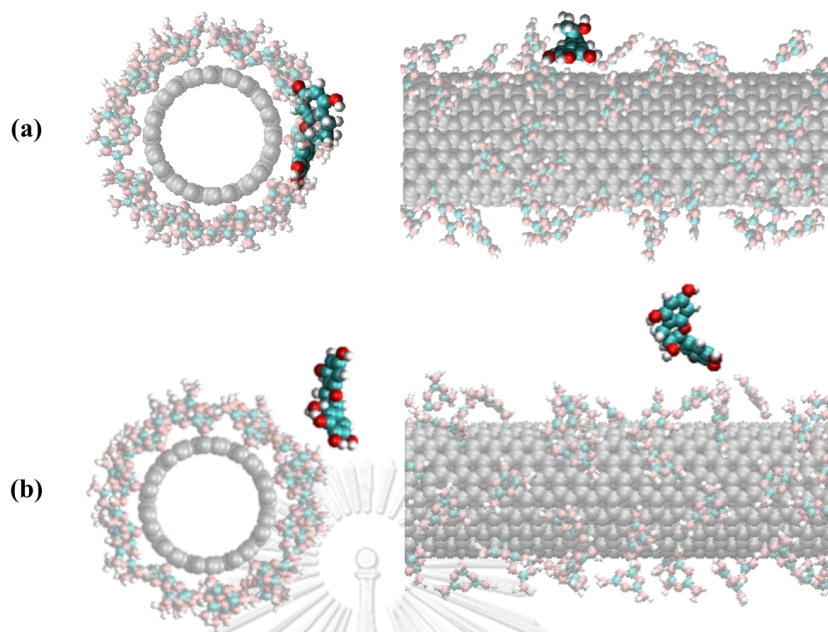


**Figure 4.9** Front view (left panel) and side view (right panel) of simulation snapshots for (a) EGC adsorbed on MA/CNT at 9 ns and (b) EGC desorbed from MA/CNT at 10 ns. Water molecules are not shown for clarity. The molecules of EGCG and EGC are highlighted and amine-functionalized CNT is transparent.

#### 4.2.2 Adsorbed morphology of EGCG and EGC on amine-functionalized CNT

##### 4.2.2.1 Simulation snapshots of ten EGCG or EGC molecules on amine-functionalized CNT

**Figure 4.** shows front view simulation snapshots of EGCG (left panel) and EGC (right panel) on to various amine-functionalized CNT at equilibrium condition. Both of EGCG and EGC are preferable to adsorb on surface of EDA/CNT and TETA/CNT more than MA/CNT. The steric hindrance structure of heteroaromatic in MA prevents EGCG and EGC adsorption. In addition, EGCG or EGC are slightly adsorbed onto surface of EDA/CNT more than TETA/CNT. This result confirm about EDA/CNT is the best adsorbent for phenolic adsorption. EGC shows the better adsorption than EGCG on EDA/CNT surface. Owing to EGC is planar molecule and can be easily penetrated to amine layer, especially EDA, which many empty sites for adsorption. Thus, it is found that EGC molecules form a monolayer. EGCG with large molecular

structure and containing more hydroxyl group than EGC, tends to agglomerate next to the layer of amine functionalized CNT.

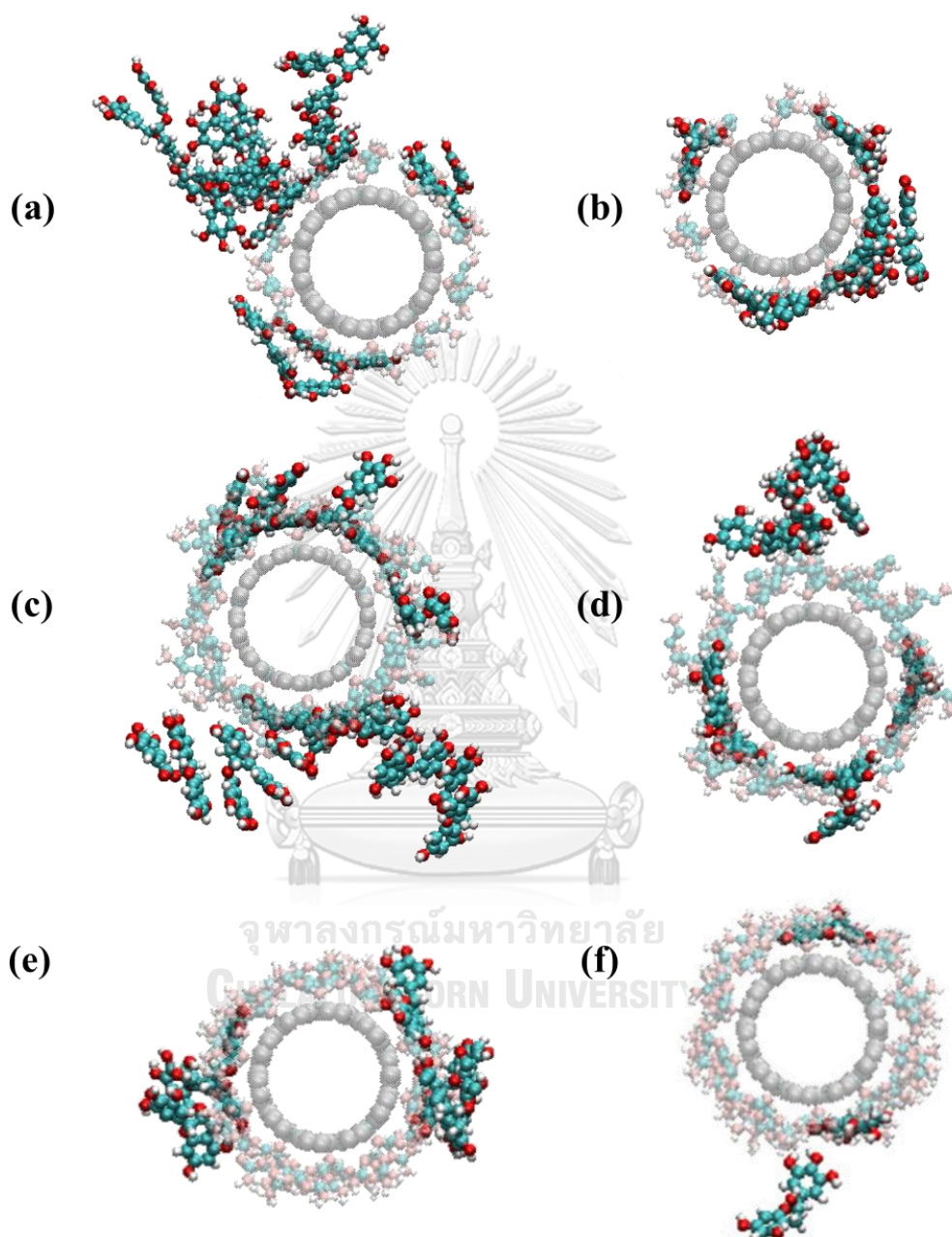


**Figure 4.10** Front views of representation simulation snapshots of 10 molecules of EGCG (left panel) and EGC (right panel) adsorb on surface of (a, b) EDA/CNT, (c, d) TETA/CNT and (e, f) MA/CNT. Water molecules are not shown for clarity. The molecules of EGCG and EGC are highlighted. All of amine functionalized CNT is transparent.

#### 4.2.2.2 The radial density profile of EGCG or EGC

The structural observations of EGCG and EGC are quantified by calculating density distributions from the center of mass of EDA, TETA, and MA that grafted on CNT surface as shown in **Figure 4.** The density profiles of EDA show the highest intensity at  $0.0013 \text{ atom}/\text{\AA}^3$  and  $0.0018 \text{ atom}/\text{\AA}^3$  for EGC and EGCG, respectively. In addition, the density distribution of EGCG shows the multiple aggregation that clearly observed in range of 8 to 10  $\text{\AA}$  and 10 to 14  $\text{\AA}$ . EGC is also provided the aggregation as a monolayer adsorption, that be showed in range of 3 to 6  $\text{\AA}$ .

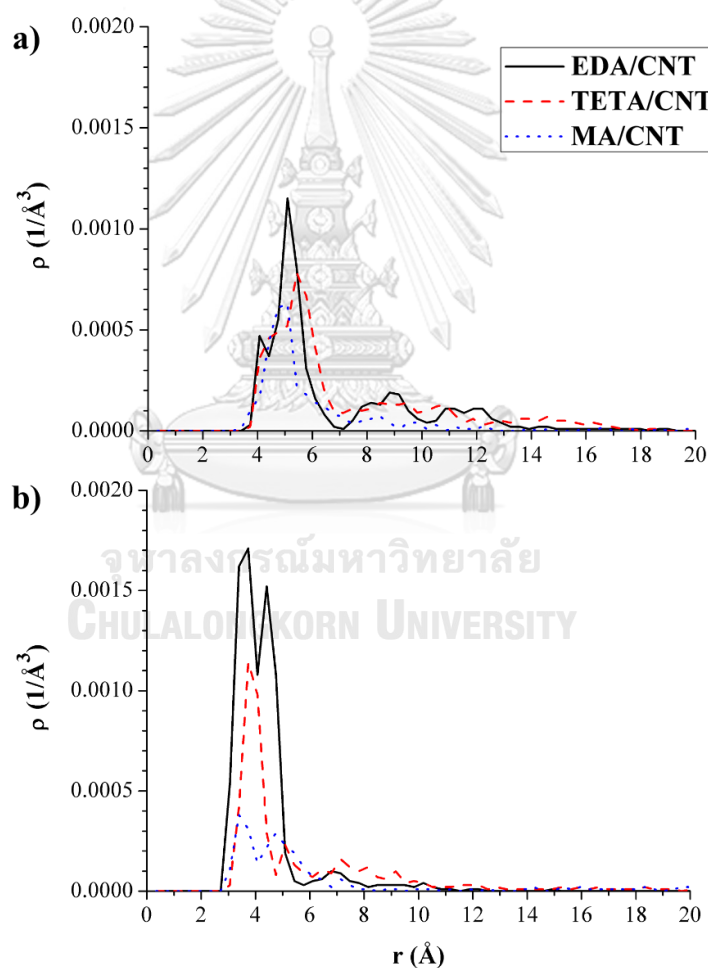


**Figure 4.11** Atomic density profiles of (a) EGCG, (b) EGC on surface of amine functionalized CNT. The black-solid, red-dashed and blue dot lines represent the results obtained from EDA/CNT, TETA/CNT and MA/CNT, respectively

The atomic density profiles between the center of mass of EGC or EGCG and EDA functionalized CNT are showed in **Figure 4.** EGCG and EGC are mostly penetrated to EDA layer in different position at 6 Å and 4 Å, respectively. EGC can be transfer inside the amine layer that deeper than EGCG.

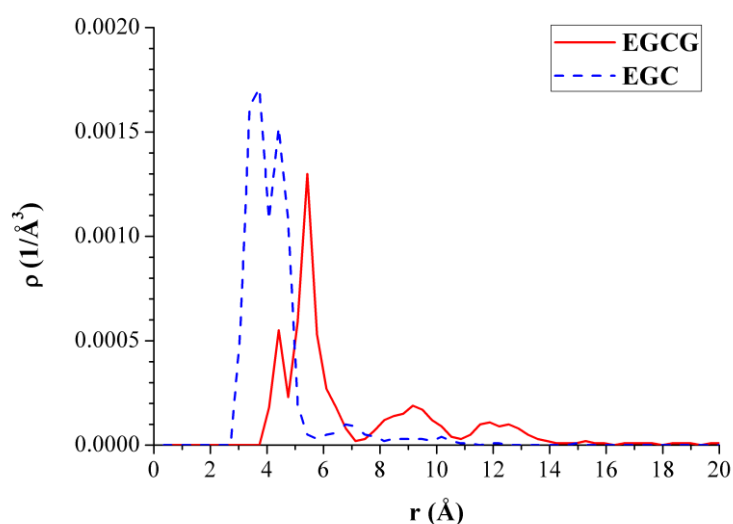


**Figure 4.12** Atomic density profiles of EGCG and EGC on surface of EDA/CNT. The red-solid and blue dot lines represent the results obtained from EGCG and EGC, respectively.

The morphology of EGCG and EGC aggregates differently on amine functionalized CNT. The chemical structures of phenolic compound are categorized to bicyclic and cyclic segment and shown in **Figure 4.** EGCG is large molecule and can be classified into three segments: bicyclic, cyclic A and cyclic B. EGC has two parts containing bicyclic and cyclic.

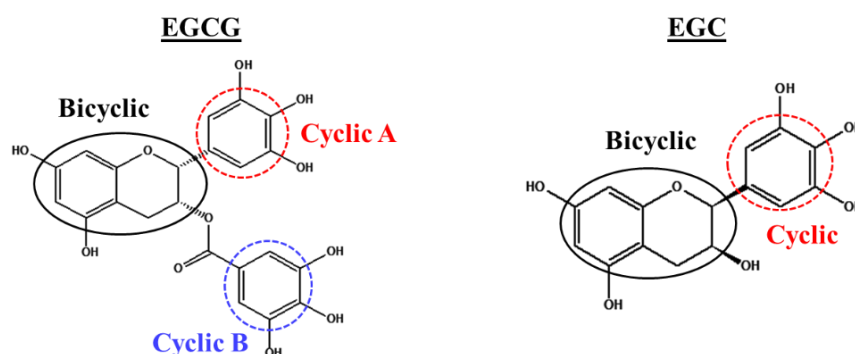


**Figure 4.13** The segment of chemical structures of EGCG and EGC.

The atomic density profiles were calculated from the center of mass of amine molecule to each segment of EGCG or EGC in radial dimension and shown in **Figure 4.4** and **Figure 4.5**.

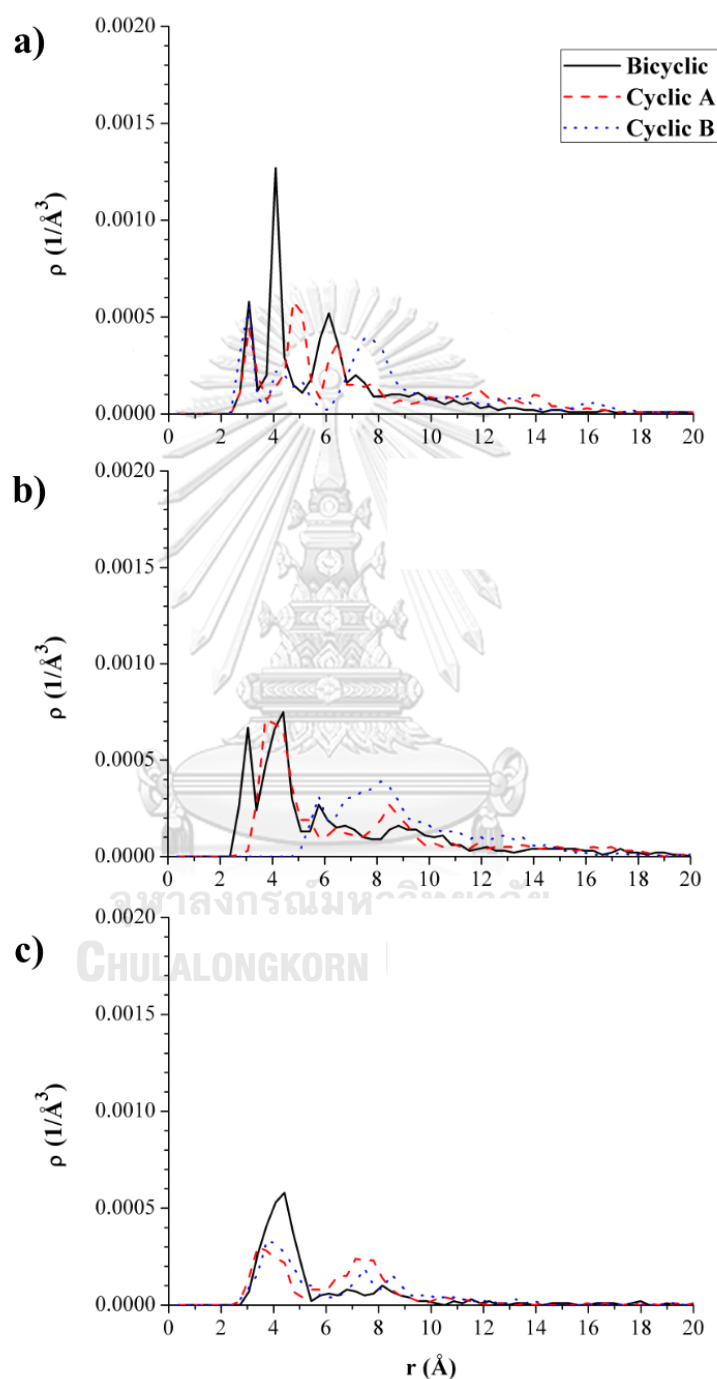


**Figure 4.4** Atomic density profiles between the structure segments in EGCG molecule and amine functionalized CNT: (a) EDA/CNT, (b) TETA/CNT and (c) MA/CNT. The black-solid, red-dashed and blue dot lines represent the results obtained from bicyclic, cyclic A and cyclic B, respectively

**Figure 4.4** shows the atomic density profiles of structure parts in EGCG. The result is hard to explain due to various peak types in many positions. EGCG show the complicate adsorption with many conformations around surface of absorber. Firstly, the adsorbed EGCG on EDA/CNT was considered and it provides the highest strong peak of bicyclic at 4 Å that be higher than cyclic A (5 Å) and cyclic B (7.5 Å). Therefore, EGCG is generally point bicyclic in to adsorb EDA/CNT. Simultaneously, EGCG can be analyzed bicyclic, cyclic A and cyclic B at the same location at 3 Å. Some molecule of EGCG has already penetrated in to EDA layer with all of segments. Second, TETA/CNT, the peaks of bicyclic and cyclic A show the highest position in range of 2 to 5 Å, measure from CNT surface. However, the peak of cyclic B is observed higher than 5 Å. The orientation of EGCG, in case of long chain amine molecule, prefer to use bicyclic and cyclic A to absorb on the surface but point out cyclic B to bulk solution because of dense packing formation of TETA/CNT. Finally, MA/CNT, all parts of EGCG are mainly absorbed at the same position around 4 Å. However, there are found some peaks of cyclic A and cyclic B at over than 7 Å. Consequently, EGCG is mostly penetrated to adsorb on free space in MA layer.

The atomic density profiles can be concluded that EGCG is used bicyclic segment to penetrate inside amine layer follow by cyclic A and cyclic B. In addition, the space area in amine layer is also affected to EGCG adsorption. If amine layer has more area, EGCG can be adapted the conformation to adsorb on amine layer, for example the adsorption of EGCG on surface of EDA/CNT.

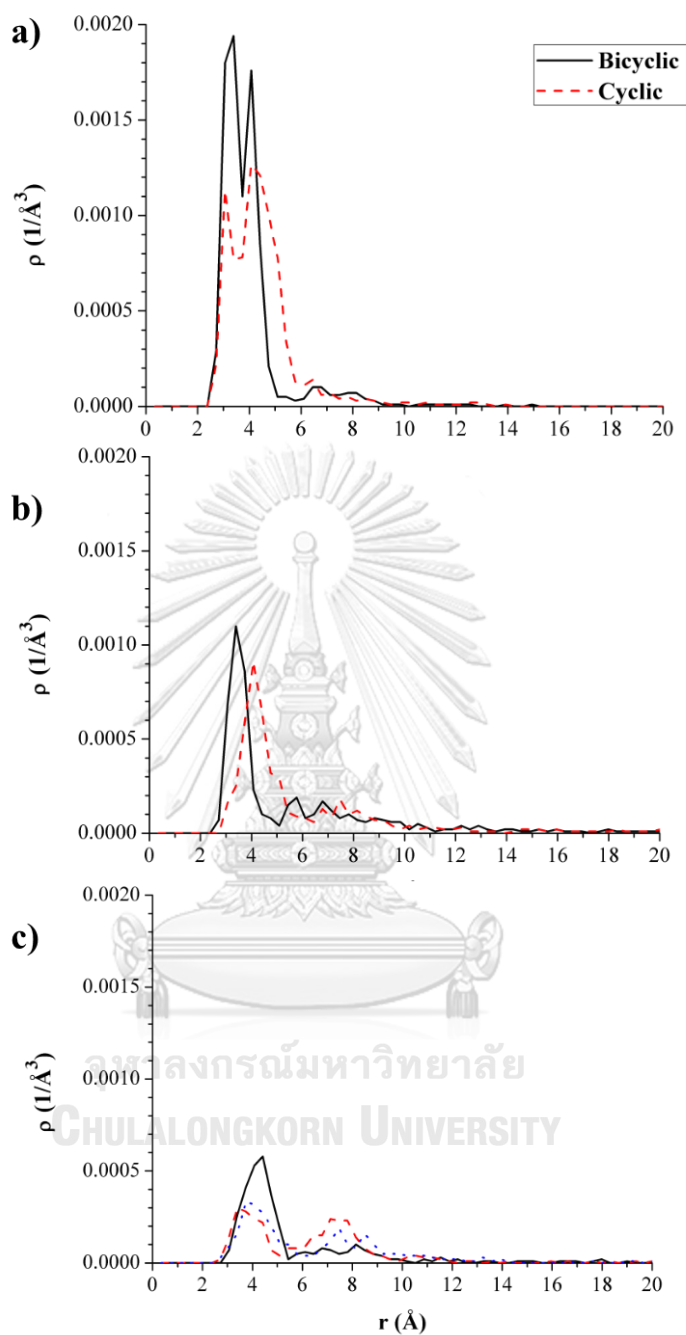


**Figure 4.5** Atomic density profiles between the structure parts in EGC molecule: molecule and amine functionalized CNT: (a) EDA/CNT, (b) TETA/CNT and (c) MA/CNT. The black-solid, red-dashed and blue dot lines represent the results obtained from bicyclic, cyclic A and cyclic B, respectively.



**Figure 4.5** shows the atomic density profiles of structure parts in EGC. EDA/CNT and TETA/CNT provide the same information. The bicyclic segment of EGC is closely adsorbed to the surface of amine functionalized CNT more than cyclic and showed the strongest peak of bicyclic and cyclic peak at 3 Å and 4 Å, respectively. Moreover, some molecule of EGC uses both bicyclic and cyclic segment to adsorb on EDA surface. The EGC adsorption on MA/CNT provides the same location of bicyclic and cyclic segment in range of 2 to 6 Å. Therefore, EGC and EGCG are generally used bicyclic segment to penetrate inside of amine layer.

#### 4.2.2.3 Radial distribution function (RDF)

The radial distribution function (RDF) is a statistical probability function to find amount of determine particle in a shell ( $dr$ ) at the distance ( $r$ ) of reference atom [31] as shown in **Figure 4.6** and defined in **Equation (12)**.

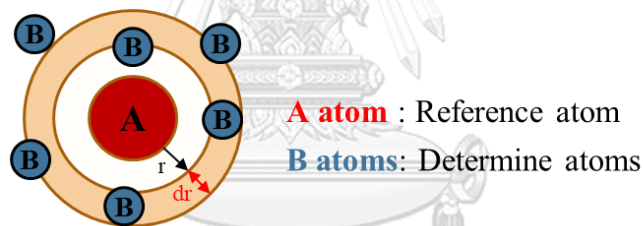


**Figure 4.6** Radial distribution function's definition

$$RDF = \frac{\rho_r}{\rho_t} = \frac{n_B}{4\pi r^2 \Delta r} \quad (12)$$

$$\rho_t = \frac{N_B}{V}$$

where  $\rho_r$  = Atomic density of determine atom at distant  $r$

$\rho_t$  = Total atomic density of determine atom

$n_B$  = Amount of determine atom in range of  $\Delta r$

$N_B$  = All determine atom at distant ( $r$ )

$V$  = Volume of spherical radius ( $r$ ) that measures from the reference atom



The RDF results were calculated to investigate the distance between various segments of phenolic compound and nitrogen atoms in EDA/CNT. **Figure 4.7** shows N1 (black color) and N2 (red color). N1 is nitrogen atom which close to CNT surface while N2 is nitrogen atom that extent to water.

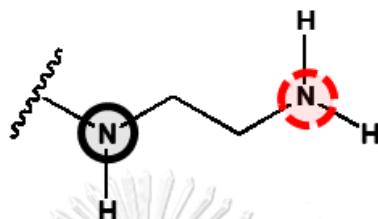


*Figure 4.7 The nitrogen atoms in EDA molecule.*

**Figure 4.18** (a) and (b) shows the RDF plot between the segments (bicyclic, cyclic A and cyclic B) of EGCG and N1, and N2, respectively. The first peak represents the shortest distance between nitrogen atom and each segment, meaning that the EGCG segment interacts with the nitrogen atom of amine. In **Figure 4.18** (a), the bicyclic of EGCG showed strongest first peak at 4 Å, representing the bicyclic segment adsorb close to N1 atom. On the other hand, RDF plot between EGCG and N2 shows similar peak intensity for all EGCG segments. These results confirm that the bicyclic of EGCG interacts with N1 of EDA molecule via hydrogen bonding. More information of hydrogen interaction of phenolic compounds and amine molecules are shown in Appendix.

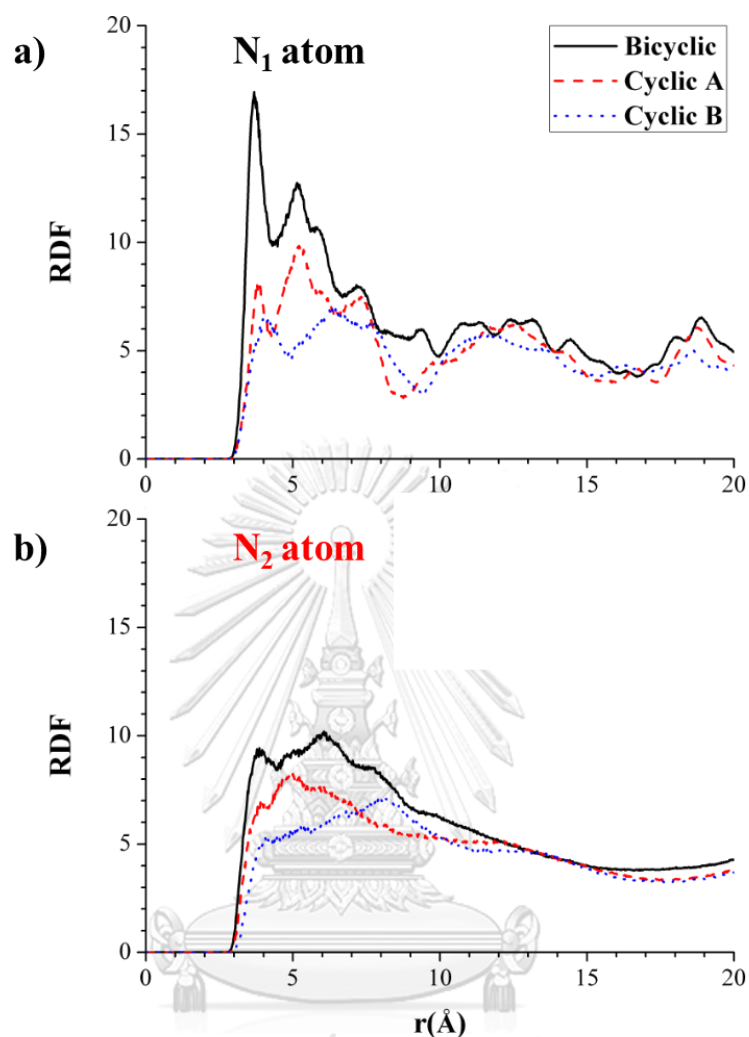


**Figure 4.8** Radial distribution function between structure segments of EGCG and nitrogen atom in EDA: (a) N1 and (b) N2. The black-solid, red-dashed and blue dot lines represent the results obtained from bicyclic, cyclic A and cyclic B, respectively.

**Figure 4.9** (a) and (b) shows the RDF plot between the segments (bicyclic and cyclic) of EGC and N1, and N2, respectively. The bicyclic of EGC showed strongest first peak at 4 Å. Nevertheless, the cyclic of EGC is close to N2 position. These results confirm that the bicyclic of EGC interacts with N1 of EDA molecule while cyclic of EGC interact with N2 atom of EDA.

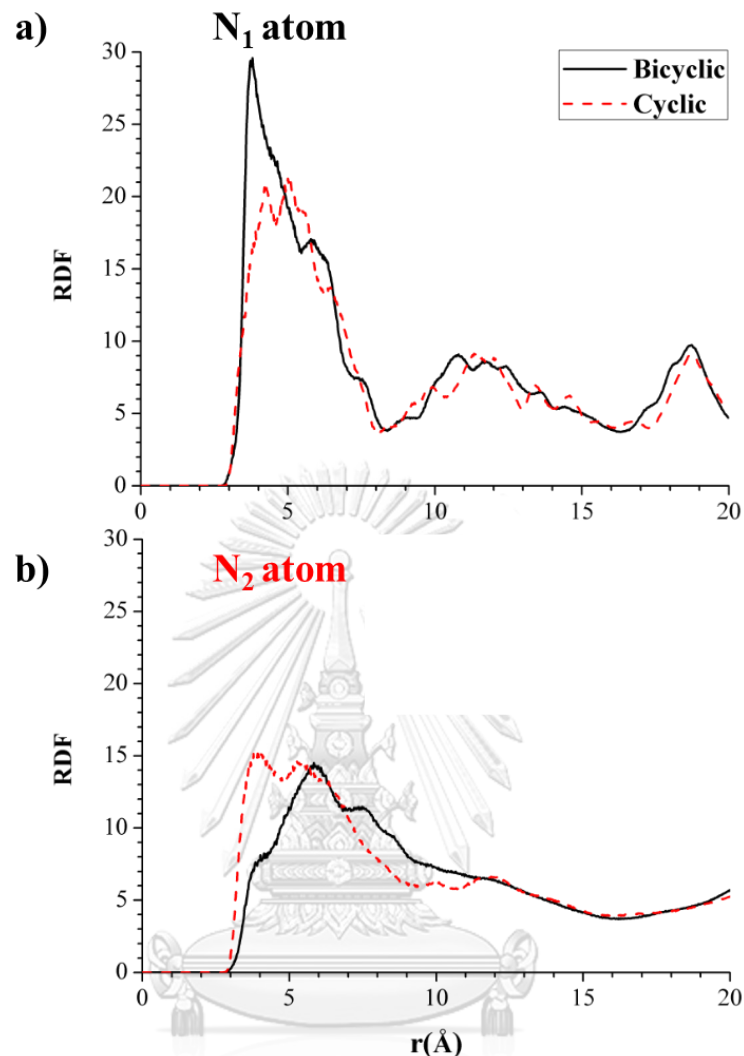


**Figure 4.9** Radial distribution function between structure segments of EGC and nitrogen atom in EDA molecule: (a) N1 and (b) N2. The black-solid, red-dashed and blue dot lines represent the results obtained from bicyclic, cyclic A and cyclic B, respectively.

#### 4.2.2.4 Binding energy ( $E_{binding}$ )

The binding energy ( $E_{binding}$ ) is input energy required to separate the conjugate pair of interesting molecule that can be defined as the opposite force from the adsorption energy as shown in **Equation (13)**.

$$E_{binding} = -E_{adsorption} \quad (13)$$

The adsorption energy ( $E_{adsorption}$ ) between phenolic molecules and amine functionalized CNT system in water solution were adapted from Yue Ma and co-worker [32]. It's showed in **Equation (14)**

$$E_{adsorption} = E_{total} - (E_{amine/CNT} + E_{phenolic\ compound}) \quad (14)$$

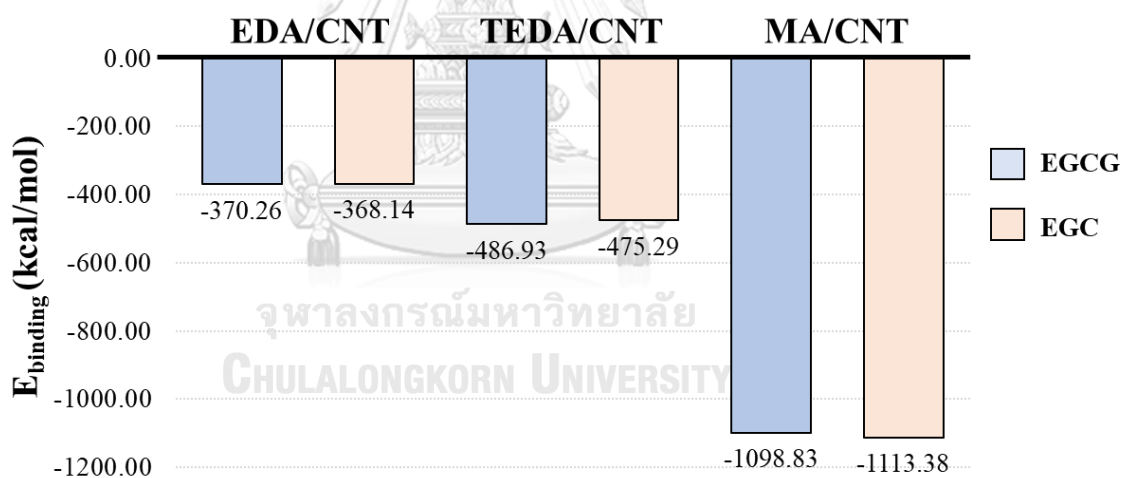
where  $E_{total}$ ,  $E_{amine/CNT}$  and  $E_{phenolic\ compound}$  are the energy parameter of system with ten molecules of EGCG or EGC adsorb on amine functionalized CNT surface, system of pure amine graft CNT and system of ten molecules of EGCG or EGC in water, respectively.

The large binding energy (or low value of adsorption energy) means stronger affinity and stability of adsorbed phenolic compound onto the layer of amine, functionalized CNT. The detail of binding energy calculation present in **Table 4.3**. The equilibrium state of adsorbed ten molecules of phenolic compound on amine-functionalized CNT in water solution were simulated to obtain  $E_{total}$ . Then, all grafted amine on CNT surface without water were reached equilibrium and can be calculated to  $E_{amine/CNT}$ . The equilibrium systems of 10 molecules phenolic compounds in water solution are investigated to obtain  $E_{phenolic\ compound}$ . The adsorption energy and binding energy are statistic computed follow **Equation (14)** and **Equation (13)**, respectively.

**Table 4.3** Binding energy calculation

No.	Amine-functionalized CNT	Phenolic compound	$E_{total}$	$E_{amine/CNT}$	$E_{phenolic\ compound}$	$E_{adsorption}$	$E_{binding}$
			(kJ/group)				
1	EDA/CNT	EGCG	39,532,300	39,953,900	-437,151	15,551	-370.26
2		EGC	39,533,100	39,953,900	-436,262	15,462	-368.14
3	TETA/CNT	EGCG	39,538,400	39,955,100	-437,151	20,451	-486.93
4		EGC	39,538,800	39,955,100	-436,262	19,962	-475.29
5	MA/CNT	EGCG	39,636,000	40,027,000	-437,151	46,151	-1098.83
6		EGC	39,637,500	40,027,000	-436,262	46,762	-1113.38

Note that the CNT were fixed at the center of the simulation box during the course of simulation,  $E_{total}$  and  $E_{amine/CNT}$  show the positive energy for all system. These values merely affect the energy calculation (see the **Equation (14)**).

**Figure 4.20** The summarize of binding energy.

The binding energy of phenolic compounds on amine-functionalized CNT are summarized in **Figure 4.20**. The binding energy between EGCG or EGC and EDA/CNT showed the highest binding energy more than obtained from TETA/CNT and MA/CNT, respectively. EDA is a shorter amine molecule provide high performance to adsorb phenolic compound as same as the result from diffusion coefficient in **Table 4.2**. EGCG and EGC are stable adsorbed on EDA/CNT. EGC is

small molecule and less of hydroxyl groups that presents large adsorption stability. The binding energy of EGC in EDA/CNT and TETA/CNT are larger than EGCG. However, the case of MA/CNT, EGCG is more binding energy than EGC due to MA/CNT is low performance to adsorb EGCG and EGC and present EGC desorption as shown in **Figure 4.**



## Chapter 5 Conclusions

This dissertation aims to investigate the effect of various molecular structures of amines molecule on phenolic compound adsorption by MD simulation. The simulated results are divided into two parts: the structural properties of various amines, which functionalized on CNT and the adsorption behavior between phenolic compounds (EGCG and EGC) and amine-functionalized CNT.

The structural properties of three different amine affect the surface diffusion and adsorption of EGCG and EGC. EDA is a shorter amine molecule and preferably extent to bulk solution. The EDA morphology on CNT surface shows no packing and independent orientation. TETA is longer chain than EDA molecule. After grafting TETA on CNT surface, it provided unexpected result, not TETA elongates in to bulk solution but, it also prefers self-aggregation to dense packing layer. Finally, the aromatic ring's amine (MA) shows dense packing around CNT surface and prefer to symmetric orientation.

The adsorption behavior of EGCG or EGC on amine functionalized CNT are considered from surface diffusion and adsorption morphology. The surface diffusion of EGCG or EGC on amine modified surface are investigated by mean square displacement (MSD) and the diffusion coefficient (D). Their results show EDA/CNT has a lowest diffusibility of adsorbed EGCG and EGC than TETA/CNT and MA/CNT, respectively. EGCG and EGC are stable and preferable to adsorb on the surface of EDA/CNT. Because EDA, a short chain amine, is provided many empty spaces in amine packing. Thus, phenolic molecules have commonly adjusted the molecular conformation to infuse inside amine layer. MA/CNT is conversely the high values of D and MSD curve, especially EGC adsorption. EGC is non-stable adsorbed on MA/CNT surface and rapidly abandoned to bulk solution.

The adsorption morphology is determined from the simulated systems, which be combined the ten molecules of phenolic compounds adsorb on surface of amine functionalized CNT in water solution. Then, it's simulated still equilibration at simulation times more than 30 ns. Absolutely, EDA/CNT is high performance

material for EGCG and EGC adsorption more other adsorption material. EDA is a good structural morphology. However, the long chain amine (TETA), is full field covered on CNT surface with self-aggregation, shows low porosity and not be provided to adsorb phenolic compound. While, the amine group with constrain aromatic ring (MA), is obstructed morphology and inhibited the conjugating phenolic molecule to adsorb on its surface.

The adsorbed morphology of EGC on EDA/CNT surface is approximately observed nearby surface of CNT, more than EGCG. The chemical structure of EGC is planar configuration with 2 groups: bicyclic and cyclic. EGC can be easily penetrated and interacted with amine, EDA, to form monolayer. The massive phenolic compound (EGCG), combining from 3 groups: bicyclic, cyclic A and cyclic B, is generally located around amine functionalize CNT and commonly to multilayer conformation.

The radial density profile and radial density distribution are considered to explain about the aggregation of EGCG or EGC adsorption. The bicyclic segment of EGCG and EGC is the first group that could be entered inside the packing layer and interacted with nitrogen atom in graft amine. Then, the other segment can be transferred itself to blank space of amine layer. If amine-absorber has some free area space in packing layer, the phenolic compound (EGCG and EGC) are adapted structure morphology to fully adsorb in amine surface site.

Finally, the binding energy between phenolic compound and amine modified CNT is studied for confirming the overall adsorption reaction. The binding energy between EGCG and EGC on EDA/CNT are higher than obtain from TETA/CNT and MA/CNT, respectively. EDA/CNT is a best material for phenolic adsorption. The adsorbed EGC on MA/CNT is showed the lowest binding energy, corresponding to desorption of EGC from MA/CNT.



## Appendices

### 1. The supporting information for interaction calculation

In this section, the interaction calculation was present. In the potential energy function (3), Lennard-Jones potential and electrostatic interactions between pairs of atoms in a molecule can be added in non-bonded interaction parameters and definite in first and second group in **Equation (S-1)**, respectively.

$$E_{nb}(r_{ij}) = \sum_{atom\ pairs} 4\varepsilon_{ij} \left[ \left( \frac{\sigma_{ij}}{r_{ij}} \right)^{12} - \left( \frac{\sigma_{ij}}{r_{ij}} \right)^6 \right]^2 + \sum_{atom\ pairs} \frac{q_i q_j}{4\pi\varepsilon_0\varepsilon_r r_{ij}} \quad (\text{S-1})$$

Lennard-Jones (LJ) potential is closely approximately by 12-6 Lennard-Jones model and represented the London dispersion forces of 2 interesting particle. In addition, Pauli-Repulsion is combined to LJ potential as an atomic repulsion factor when particles are extremely short distances.

**Table S1.** Atom definition and non-bonded parameters.

Atom/group	Definition	mass	$\sigma$ [Å]	$\varepsilon$ [kcal mol <sup>-1</sup> ]	$\delta$ [e]
H	H bonded to nitrogen atom	1.01	1.070	0.0157	0.394
HA	H bonded to aromatic carbon	1.01	2.600	0.0150	0.152
HC	H bonded to aliphatic carbon	1.01	2.650	0.0157	0.105
HO	H in hydroxyl group	1.01	0.000	0.0000	0.450
N2	N (sp2) in amine groups	14.01	3.250	0.1700	-0.788
NC	N (sp2) in 6 membrane rings	14.01	3.250	0.1700	-0.860
C	C (sp2) in carbonyl group	12.01	3.400	0.0860	0.775
CA	C (sp2) in aromatic	12.01	3.400	0.0860	0.871
CT	C (sp3) in aliphatic	12.01	3.400	0.1094	0.179
CT2	CH <sub>2</sub> group in hydrocarbon	14.03	4.020	0.0560	0.000
O	O in carbonyl group	16.00	2.960	0.2100	-0.604
OH	O in hydroxyl group	16.00	3.070	0.2104	-0.518
OS	O in ether and ester groups	16.00	3.000	0.1700	-0.386
OW	O in TIP3P water	16.00	3.166	0.1554	-0.834
HW	H in TIP3P water	1.01	0.000	0.0000	0.417
c	C in CNT	12.01	3.400	0.0557	0.000

where  $\sigma$  and  $\varepsilon$  are the collision diameter and the well depth, respectively.

For example, we determine the Lennard-Jones (LJ) potential of nitrogen in amine molecule (N2) and oxygen of hydroxyl group in phenolic compound (OH).

Firstly,  $\sigma_{ij}$  and  $\epsilon_{ij}$  are integrated from the combining rule of Lorentz-Berthelot (4) and parameter in **Lennard-Jones** (LJ) potential is closely approximately by 12-6 Lennard-Jones model and represented the London dispersion forces of 2 interesting particle. In addition, Pauli-Repulsion is combined to LJ potential as an atomic repulsion factor when particles are extremely short distances.

**Table S1.**

$$\sigma_{N2,OH} = \frac{(\sigma_{N2} + \sigma_{OH})}{2} = \frac{(3.250 + 3.070)}{2} = 3.160 \text{ \AA}$$

$$\epsilon_{N2,OH} = \sqrt{\epsilon_{N2}\epsilon_{OH}} = \sqrt{0.1700 \times 0.2104} = 0.1891 \text{ kcal mol}^{-1}$$

Then, Lennard-Jones potential of nitrogen in amine (N2) and oxygen of hydroxyl group (OH) is calculated by using  $\sigma_{N2,OH}$  and  $\epsilon_{N2,OH}$ .

$$E_{LJ(N2,OH)}(r) = 4\epsilon_{N2,OH} \left[ \left( \frac{\sigma_{N2,OH}}{r} \right)^{12} - \left( \frac{\sigma_{N2,OH}}{r} \right)^6 \right]^2$$

$$E_{LJ(N2,OH)}(r) = 0.7564 \left[ \left( \frac{3.160}{r} \right)^{12} - \left( \frac{3.160}{r} \right)^6 \right]^2 \quad (\text{S-2})$$

So, the relationship of nitrogen in amine (N2) and oxygen of hydroxyl group (OH) is showed that, the atomic distant ( $r$ ) in **Equation (S-2)** is affected to energy force, especially, the shorter distant than cut-off values.

In addition, the electrostatic interactions are represented Dipole-Dipole interaction of 2 polar species and can be transformed potential in term of electric conversion factor ( $f$ ) as shown **Equation (S-3)**.

$$E_{coulomb}(r_{ij}) = \sum_{atom\ pairs} \frac{q_i q_j}{4\pi\epsilon_0\epsilon_r r_{ij}} \approx \sum_{atom\ pairs} f \frac{q_i q_j}{\epsilon_r r_{ij}} \quad (\text{S-3})$$

The relative dielectric constant is  $\epsilon_r$  ( $\epsilon_r$  is 1 when without reaction field) and electric conversion factor is  $f$  ( $f = (4\pi\epsilon_0)^{-1} = 332,063.574 \text{ kcal mol}^{-1} \text{ \AA e}^{-2}$ )

For example, we determine the electrostatic interactions of nitrogen in amine molecule (N2) and oxygen of hydroxyl group in phenolic compound (OH). The **Equation (S-3)** is applied with charge of N2 and OH to **Equation (S-4)**.

$$E_{c(N2,OH)}(r) \approx f \frac{q_{N2}q_{OH}}{\epsilon_r r} = 332,063.574x \frac{0.788 \times 0.518}{r} \quad (\text{S-4})$$

From the potential energy function, bonded interaction parameters consisted of bond stretching, angle bending, and dihedral torsion as demonstrated in first, second and third term of **Equation (S-5)**.

$$E_b = \sum_{bonds} \frac{a_i}{2} (r_i - r_{i0})^2 + \sum_{angles} \frac{b_i}{2} (\theta_i - \theta_{i0})^2 + \sum_{torsions} \frac{c_i}{2} [1 + \cos(n\omega_i - \gamma_i)] \quad (\text{S-5})$$

The first group of bonded interaction, the bond stretching between two interest atoms is represented by a harmonic potential and simplified to **Equation (S-6)**.

$$E_{bond}(r) = \sum_{bonds} k_b (r - b_0)^2 \quad (\text{S-6})$$

when  $k_b$  and  $b_0$  are bonding force constant and equilibrium bond length and can be showed in **Table S2**. Bond-stretching parameters.

For example, the bonding energy equation of carbon-carbon in aromatic ring in phenolic compound (EGCG and EGC) can be applied from harmonic potential as given in **(S-7)** The bond starching is departed from equilibrium, affect to bonding energy and be a cause of molecular orientation.

$$E_{CA-CA}(r) = 469 \times (r - 1.4)^2 \quad (\text{S-7})$$

$r$  is a bond length at any simulation times



**Table S2.** Bond-stretching parameters

Bond	$b_0$ [Å]	$k_b$ [kcal mol <sup>-1</sup> Å <sup>-2</sup> ]
CA-CA	1.400	469.00
CA-CT	1.510	317.00
CA-NC	1.339	483.00
CA-N2	1.340	481.00
CA-OS	1.240	480.00
CA-OH	1.364	450.00
CA-HA	1.080	367.00
CT-CT	1.526	310.00
CT-HC	1.090	340.00
CT-OS	1.240	480.00
CT-OH	1.364	450.00
C-OS	1.323	450.00
C=O	1.229	570.00
C-CA	1.409	469.00
N2-CT	1.471	367.00
N2-c	1.383	424.00
N2-H	1.010	434.00
OH-HO	0.960	553.00
OW-HW	0.957	600.40

where  $b_0$  and  $k_b$  are bond length and force constant at equilibrium

The second group in bonded interaction, the energy from angle-bending can be simplified and showed in **Equation (S-8)**. The bending angle can be changed from equilibrium angle overtimes and affected to total energy potential.

$$E_{angle}(\theta_i) = \sum_{angles} \frac{k_\theta}{2} (\theta_i - \theta_0)^2 \quad (\text{S-8})$$

where  $\theta_0$  and  $k_\theta$  are bond-angle at equilibrium and angle potentials constant as can be observed in **Table S3**.

For example, the equation of bending angle in aromatic ring of phenolic compound (CA-CA-CA) can be determined to **Equation (S-9)**.  $\theta$  is the bending angle in any simulation times in radius unit.

$$E_{angle}(\theta) = \frac{k_\theta}{2} (\theta - \theta_0)^2 = \frac{126}{2} x (\theta - (120x0.0175))^2 = 63x(\theta - 2.09)^2 \quad (\text{S-9})$$

**Table S3.** Angle-bending parameters

Angle	$\theta_0$ [deg]	$k_\theta$ [kcal mol <sup>-1</sup> rad <sup>-2</sup> ]
CA-CA-CA	120.0	126.00
CA-CA-C	120.0	126.00
CA-CA-HA	120.0	100.00
CA-CA-OH	120.0	140.00
CA-OH-HO	113.0	100.00
CA-CA-CT	120.0	140.00
CA-CT-CT	114.0	126.00
CA-CT-HC	109.5	100.00
CA-CA-OS	125.0	160.00
CA-CT-OS	109.5	100.00
CA-OS-CT	109.5	120.00
CA-NC-CA	120.0	140.000
CA-N2-H	120.0	100.000
CA-C-O	115.0	160.00
CA-C-OS	120.0	140.00
CT-CT-CT	109.5	80.00
CT-CT-HC	109.5	100.00
CT-CT-OH	109.5	100.00
CT-OH-HO	108.5	110.00
CT-CT-OS	109.5	100.00
CT-CT-N2	109.7	160.00
CT-N2-H	118.0	100.00
CT-N2-CT	109.5	100.00
CT-OS-C	109.5	120.00
c-N2-H	120.0	100.00
c-N2-CT	121.9	100.00
NC-CA-NC	120.0	140.000
NC-CA-N2	119.3	140.000
OS-C-O	125.0	160.00
H-N2-H	120.0	70.000
H-N2-CT	118.0	100.00
HC-CT-HC	109.5	70.00
HC-CT-OH	109.5	100.00
HC-CT-OS	109.5	100.00
HW-OW-HW	104.5	150.10

where  $\theta_0$  and  $k_\theta$  are bond-angle at equilibrium and angle potentials constant

The final group from bonded interaction is dihedral torsion. The dihedral torsion **Equation (S-10)** is commonly transformed to **Equation (S-11)** by using Ryckaert-Bellemans (RB) dihedral function.

$$E_{dihedral}(\omega_i) = \sum_{\text{torsions}} \frac{c_i}{2} [1 + \cos(n\omega_i - \gamma_i)] \quad (\text{S-10})$$

$$E_{dihedral}(\omega) = \frac{1}{2} [F_1(1 + \cos(\omega)) + F_2(1 - \cos(2\omega)) + F_3(1 + \cos(3\omega)) + F_4(1 - \cos(4\omega))] \quad (\text{S-11})$$

$$c_0 = F_2 + \frac{1}{2}(F_1 + F_3), c_1 = \frac{1}{2}(-F_1 + 3F_3), c_2 = -F_2 + 4F_4,$$

$$c_3 = -2F_3, c_4 = -4F_4$$

To solve **Equation (S-11)**, we must firstly calculate the RB dihedral constant from **Table S4**.

**Table S4.** Dihedral torsion parameter

Dihedral	$c_0$	$c_1$	$c_2$	$c_3$
	[kcal mol <sup>-1</sup> ]			
CA-CA-CA-CA	30.334	0	-30.334	0
CA-CA-CA-CT	30.334	0	-30.334	0
CA-CA-CA-C	30.334	0	-30.334	0
CA-CA-CA-OS	30.334	0	-30.334	0
CA-CA-CA-OH	30.334	0	-30.334	0
CA-CA-CA-HA	30.334	0	-30.334	0
CA-CA-CT-CT	0	0	0	0
CA-CA-CT-HC	0	0	0	0
CA-CA-C-O	30.334	0	-30.334	0
CA-CA-C-OS	30.334	0	-30.334	0
CA-CA-OH-HO	7.5312	0	-7.5312	0
CA-CA-OS-CT	8.7864	0	-8.7864	0
CA-CT-CT-HC	0.6508	1.9525	0	-2.6034
CA-CT-OS-CA	1.6039	4.8116	0	-6.4155
CT-CT-CT-CH	0.6694	2.0083	0	-2.6778
CT-CT-CT-CA	0.6508	1.9525	0	-2.6034
CT-CT-CT-OS	0.6508	1.9525	0	-2.6034
CT-CT-OS-CA	1.6039	4.8116	0	-6.4155
CT-CT-OS-C	4.9497	8.1546	0	-6.4099
CT-CA-CA-HA	30.334	0	-30.334	0

**Table S5.** (cont.) Dihedral torsion parameter

Dihedral	$c_0$	$c_1$	$c_2$	$c_3$
	[kcal mol <sup>-1</sup> ]			
CT-CT-N2-c	10.0416	-3.3472	16.736	-6.6944
CT-CT-N2-H	0.65084	1.95253	0	-2.60338
CT-CT-N2-CT	0.65084	1.95253	0	-2.60338
O-C-CA-CA	30.334	0	-30.334	0
O-C-OS-CT	28.4512	5.8576	-22.5936	0
O-C-OS-CT	28.4512	5.8576	-22.5936	0
OH-CA-CA-OH	30.334	0	-30.334	0
OS-CA-CA-CT	30.334	0	-30.334	0
OS-CT-CT-CA	0.6508	1.9525	0	-2.6034
OS-CT-CT-HC	1.046	-1.046	0	0
OS-CT-CT-OS	0.6025	1.8075	9.8324	-2.41
OS-C-CA-CA	30.334	0	-30.334	0
N2-CA-NC-CA	12.552	0	-12.552	0
N2-CT-CT-N2	0.65084	1.95253	0	-2.60338
NC-CA-N2-H	20.0832	0	-20.0832	0
NC-CA-N2-H	20.0832	0	-20.0832	0
HC-CT-CT-OS	1.046	-1.046	0	0
HC-CT-CT-HC	0.6276	1.8828	0	-2.5104
HC-CT-OS-CA	1.6039	4.8116	0	-6.4155
HA-CA-CA-OH	30.334	0	-30.334	0
HA-CA-CA-OS	30.334	0	-30.334	0

where  $C_0$ ,  $C_1$ ,  $C_2$ , and  $C_3$  are constant parameter in RB dihedral, ( $C_4 = 0$ )

For example, the equation of dihedral torsion in aromatic ring of phenolic compound (CA-CA-CA-CA) is calculated from the RB dihedral constant. the constant values of  $C_1$ ,  $C_3$ , and  $C_4$  equal to 0, and give  $F_1$ ,  $F_3$  and  $F_4$  parameters to 0. Therefore,  $F_2$  parameter is 30.334 kcal mol<sup>-1</sup>.

$$-2F_3 = 0, -4F_4 = 0 \text{ and } \frac{1}{2}(-F_1 + 3F_3) = 0 \gg F_1, F_3, F_4 = 0$$

$$F_2 + \frac{1}{2}(F_1 + F_3) = 30.334 \gg F_2 = 30.334$$

After that, the RB dihedral function can be used to solve equation and be provided in **Equation (S-12)**



$$\begin{aligned}
 E_{dihedral}(\omega) &= \frac{1}{2} [30.334x(1 - \cos(2\omega))] = 15.167x(1 - \cos(2\omega)) \\
 &= 15.167x(1 - (2\cos^2(\omega) - 1)) = 15.167x(2 - 2\cos^2(\omega))
 \end{aligned}
 \tag{S-12}$$

## 2. The interaction of phenolic compounds and amine molecules

The phenolic compounds can be adsorbed on porous materials by intermolecular force between hydroxyl groups in phenolic compounds and chemical structure of solid sorbents. In this dissertation, we use amine functionalized as a solid sorbent.

The structure of amine compound is comprised the nitrogen atom with a lone pair of electrons which high polarity atom. Normally the structure of amines are classified to three types namely, primary, secondary and tertiary follow the numbering of replacing alkyl or aryl groups [33]. The primary and secondary amine molecule are often engaged the intermolecular force as a result of hydrogen bonding between the lone pair on nitrogen atom with negative electronegativity and the slightly positive changed of hydrogen atom in another molecule [34]. On the other hand, tertiary amines are not observed the intermolecular association due to the absence of free hydrogen atoms in amine group [34].

The amine molecules can be formed stronger hydrogen bond with alcohol because a higher positive polarity of hydrogen atom in hydroxyl group. Moreover, not only hydrogen bonds can form between nitrogen atom of amines and the hydrogen atom in another adsorbed compound but also van der Waals forces, dipole-dipole, hydrophobic interactions, and/or  $\pi$ - $\pi$  stacking can be formed as minor molecular interaction.

The hydrogen bonding interaction is special type of dipole-dipole attraction as a weak force from hydrogen atom bonded to a strongly electronegative atom is interacted with the lone pair of electrons on another electronegative atoms as shown in **Figure S1**.

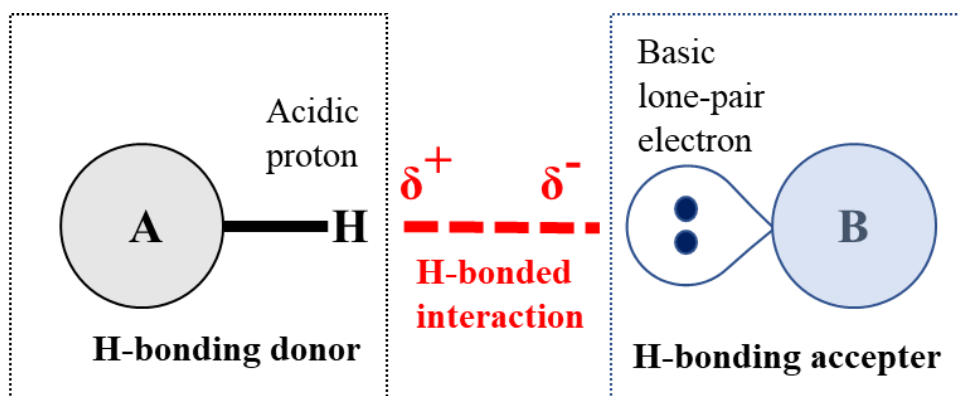


*Figure S1. The diagram of the potential hydrogen bonds formation.*

Atoms A and B are referred to periodic atoms which its electronegativity is greater than that hydrogen atom for example fluorine (F), oxygen (O) and nitrogen (N). In this dissertation, the hydrogen bonding distance between amine and hydroxyl group, which measure distant form nitrogen atom to oxygen atom, is a function of the degree of positive charge on acidic proton [35].

The hydrogen bonding distant was proposed by Kollman and Allen [35] and showed the result in 2 cases. The first case, the hydrogen atom from amine functional group is proton donor to donate hydrogen atom to lone-pair of oxygen atom in hydroxyl group, the hydrogen bonding distant is 3.41 Å. On the other hand, the second case, the nitrogen of amine as a hydrogen acceptor from hydroxyl group, the distant is 3.12 Å.

The angle of hydrogen bonding interaction can be defined follow **Figure S2** [36]. In case of angle on acceptor atom ( $\widehat{CaAD}$ ), the angle is range of 90 to 180 degrees. while the angle on hydrogen donor atom ( $\widehat{AHD}$ ) is range of 140 to 180 degrees.

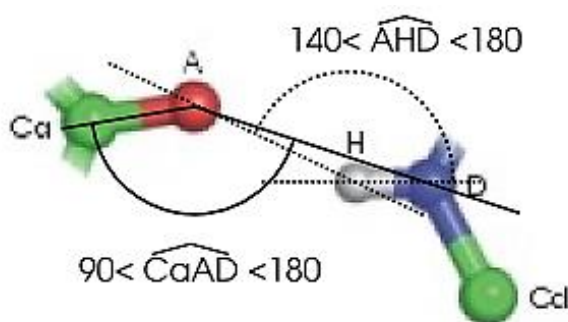


*Figure S2. The Hydrogen bond angle assessment [36].*

where Ca and A are carbon link to the acceptor atom and acceptor atom, respectively.

Cd, D and H are carbon link to the donor atom, donor atom and hydrogen atom, respectively

The adsorption behavior of phenolic compound, both of EGCG and EGC, are likely adsorbed onto nitrogen atom of EDA/CNT. The example of bond distance and angle in the hydrogen bonding interaction between EGC and EDA graft on CNT surface are showed in **Figure S3** and **Figure S4**, respectively.

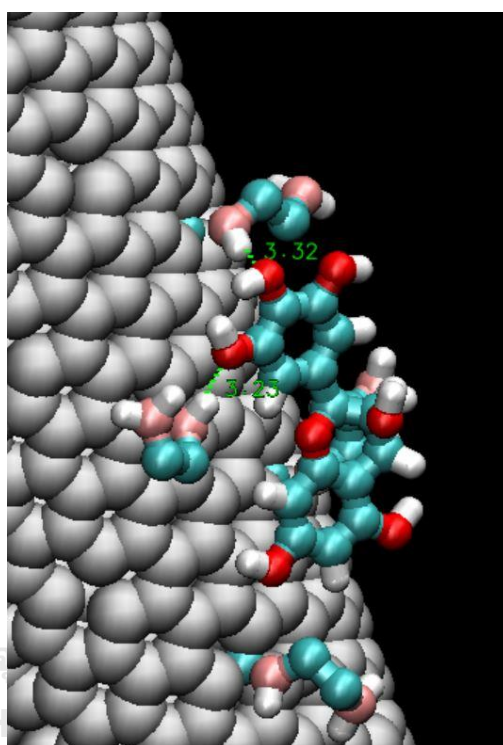


**Figure S3.** The hydrogen bonding distance of EGC adsorb on EDA/CNT surface.

In this research, **Figure S3** shows the example snapshot of hydrogen bonding distance, which measured from nitrogen atom in EDA and oxygen atom in hydroxyl group of EGC. The distance values are 3.23 and 3.32 Å, that values are nearly the result from Kollman and Allen experiment. Thus, we conclude that, hydrogen bonding is a major interaction for EGCG and EGC adsorbed on amine molecule.

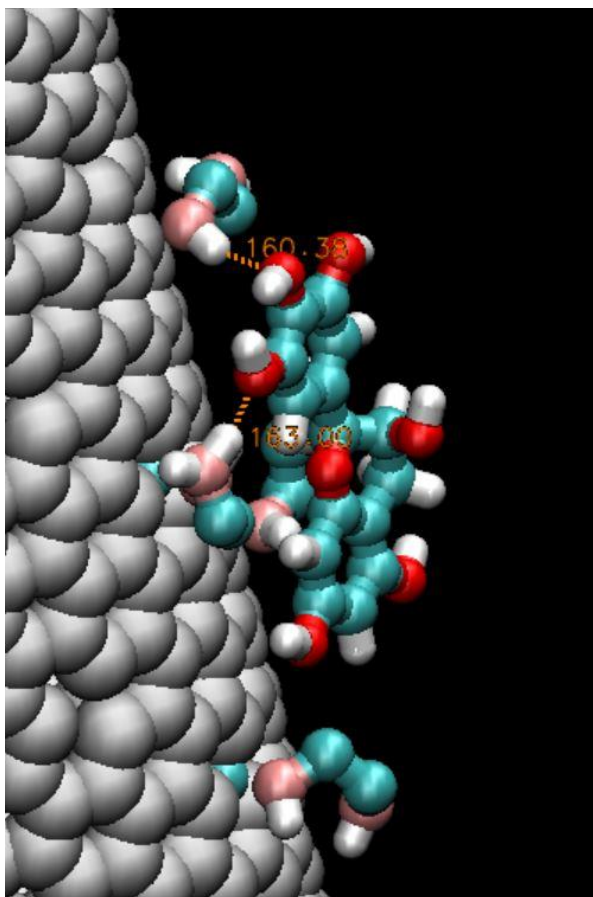


*Figure S4. The hydrogen bonding angle of EGC adsorb on EDA/CNT surface.*

**Figure S4** shows the angle of hydrogen bonding interaction that measure at hydrogen atom (AHD) which it connects to the nitrogen atom of amine (donor atom) and interacts to oxygen of hydroxyl group in EGCG (accepter atom). Their angles in this simulation snapshot are 160.33 and 163.00 degrees that confirm main interaction between phenolic compound and amine molecules is hydrogen bonding.

### 3. The details of all simulation

The information details of all simulation systems are presented in **Table S6**.

**Table S6.** All details of simulation system

No.	CNT		Graft amines		Phenolic compounds		Number of waters	Steps	dt (ps)	Simulation times (ns)
	Type	number	Type	Number	Type	Number				
1	CNT	750	EDA	50	-	-	13519	10M	0.002	20
2	CNT	750	TETA	50	-	-	13351	10M	0.002	20
3	CNT	750	MA	50	-	-	13424	20M	0.001	20
4	CNT	800	-	-	-	-	13684	10M	0.002	20
5	CNT	750	EDA	50	EGCG	1	13502	10M	0.002	20
6	CNT	750	TETA	50	EGCG	1	13329	10M	0.002	20
7	CNT	750	MA	50	EGCG	1	13407	20M	0.001	20
8	CNT	750	EDA	50	EGC	1	13504	10M	0.002	20
9	CNT	750	TETA	50	EGC	1	13336	10M	0.002	20
10	CNT	750	MA	50	EGC	1	13411	20M	0.001	20
11	CNT	750	EDA	50	EGCG	10	13339	30M	0.002	60
12	CNT	750	TETA	50	EGCG	10	13147	30M	0.002	60
13	CNT	750	MA	50	EGCG	10	13207	40M	0.001	40
14	CNT	750	EDA	50	EGC	10	13394	30M	0.002	60
15	CNT	750	TETA	50	EGC	10	13218	30M	0.002	60
16	CNT	750	MA	50	EGC	10	13255	40M	0.001	40
17	CNT	800	-	-	EGCG	1	13665	10M	0.002	20
18	CNT	800	-	-	EGC	1	13671	10M	0.002	20
19	CNT	800	-	-	EGCG	10	13488	10M	0.002	20
20	CNT	800	-	-	EGC	10	13534	10M	0.002	20
21	CNT	750	EDA	50	-	-	-	10M	0.002	20
22	CNT	750	TETA	50	-	-	-	10M	0.002	20
23	CNT	750	MA	50	-	-	-	20M	0.001	20
24	CNT	800	-	-	-	-	-	10M	0.002	20
25	-	-	-	-	EGCG	10	13870	5M	0.002	10
26	-	-	-	-	EGC	10	13929	5M	0.002	10

#### 4. The comparison of MSD of EGCG and EGC adsorb on all material

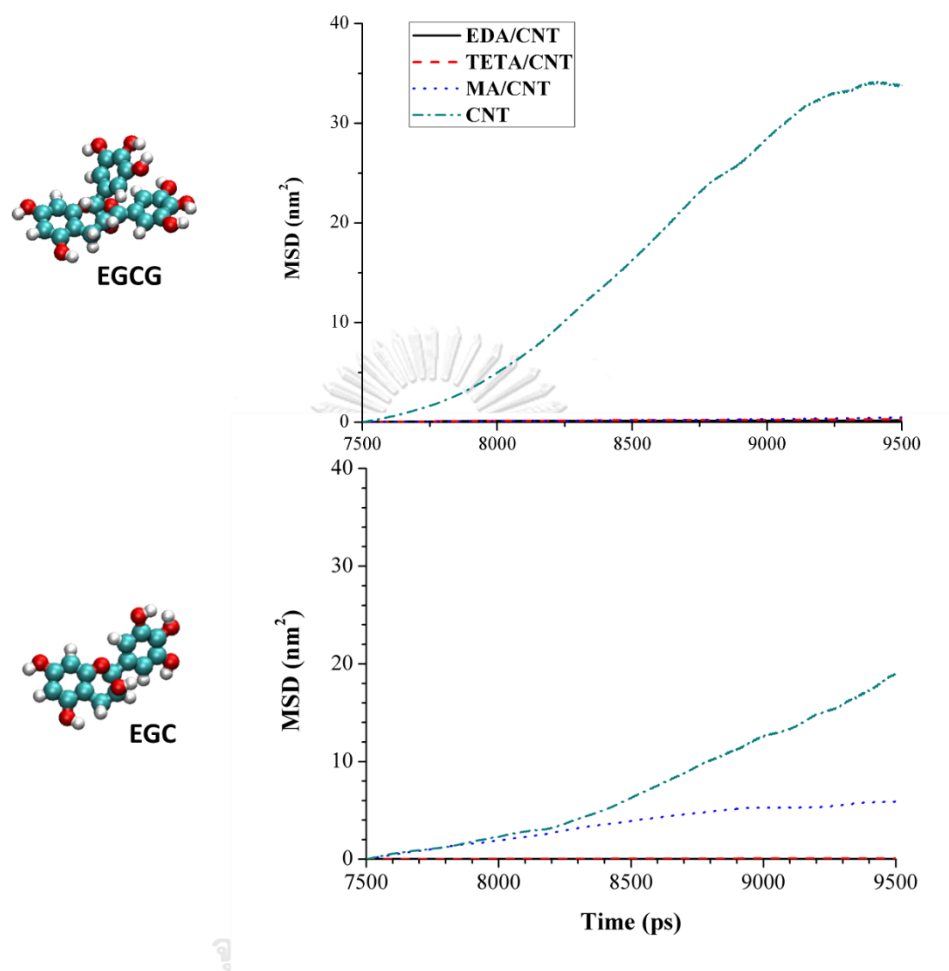


**Figure S5.** Mean-squared displacement analysis of projection from EGCG (Top panel) and EGC (Bottom panel) on amine-functionalized CNT and pure CNT.

## 5. Radial distribution function (RDF) of phenolic compounds on nitrogen of TETA

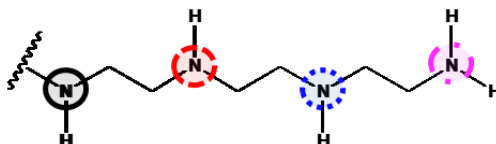


Figure S6. The nitrogen atoms in TETA/CNT.

where N1 is nitrogen atom which close to CNT surface (black cycle). N2, N3 and N4 are nitrogen atoms in amine group as shown in red, blue and pink cycle, respectively.

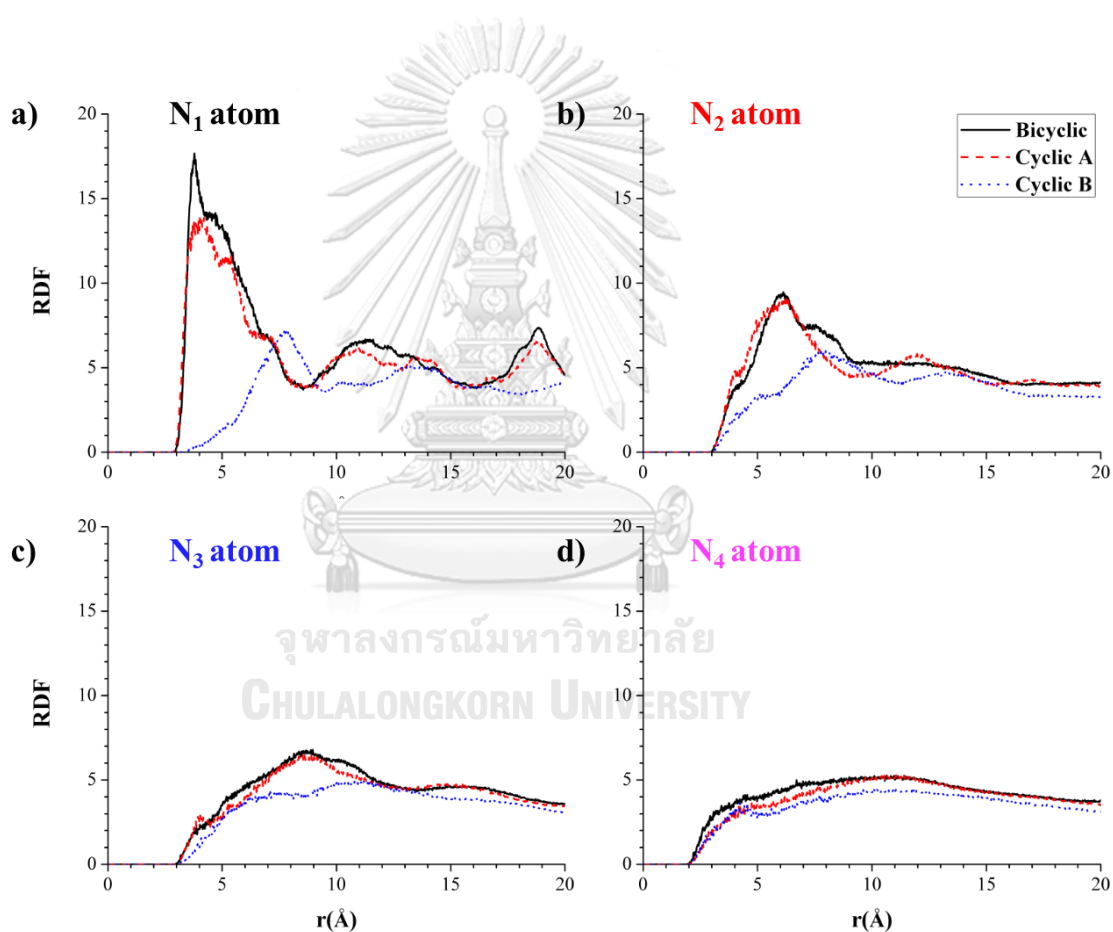
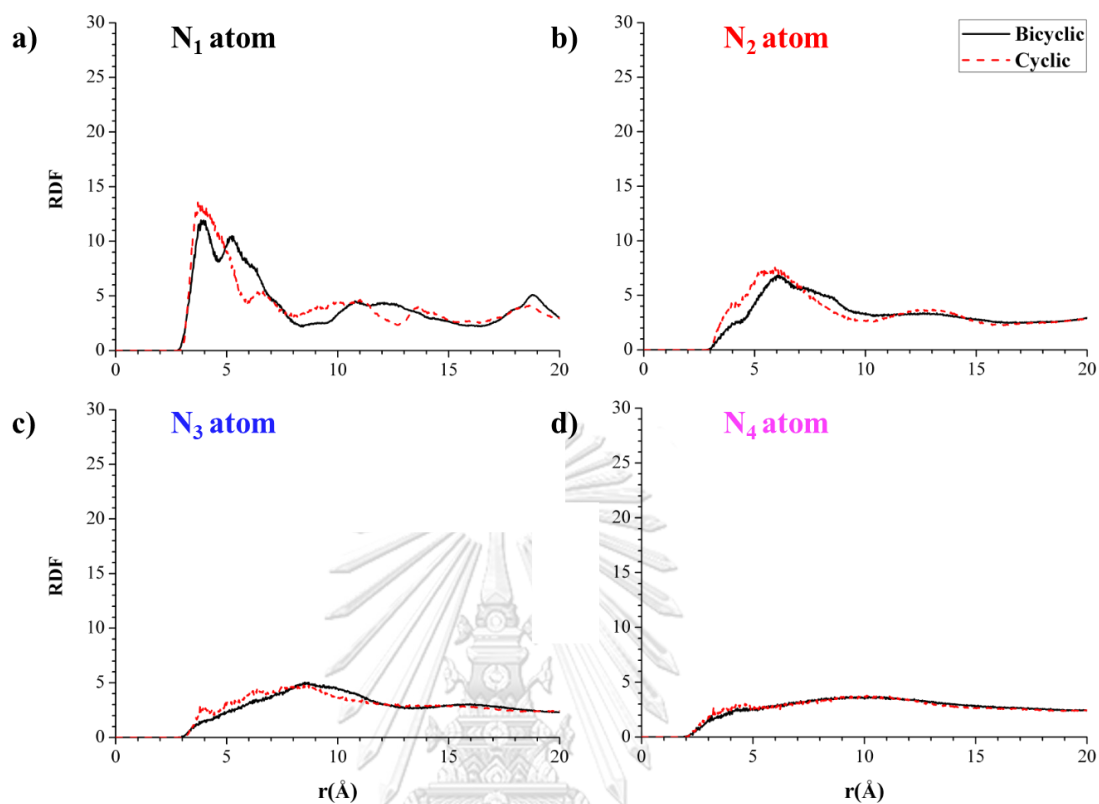


Figure S7. Radial distribution function between structure segments of EGCG molecule and nitrogen atom in TETA molecule: (a) N1, (b) N2, (c) N3, and (d) N4. The black-solid, red-dashed and blue dot lines represent the results obtained from bicyclic, cyclic A and cyclic B, respectively.



**Figure S8.** Radial distribution function between structure segments of EGC molecule and nitrogen atom in TETA molecule: (a) N1, (b) N2, (c) N3, and (d) N4. The black-solid, red-dashed and blue dot lines represent the results obtained from bicyclic, cyclic A and cyclic B, respectively.



## 6. Radial distribution function (RDF) of phenolic compounds on nitrogen of MA

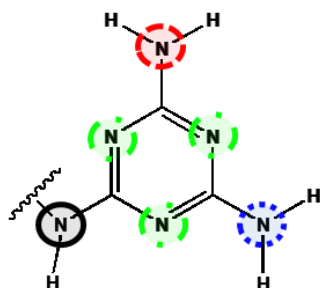


*Figure S9. The nitrogen atoms in MA/CNT.*

where N1 is nitrogen atom which close to CNT surface (black cycle). N2, N3 and N4 are aromatic nitrogen ( $N_a$ ) atoms in green cycle. N5 and N6 are nitrogen atoms in amine group as shown in red and blue cycle, respectively.

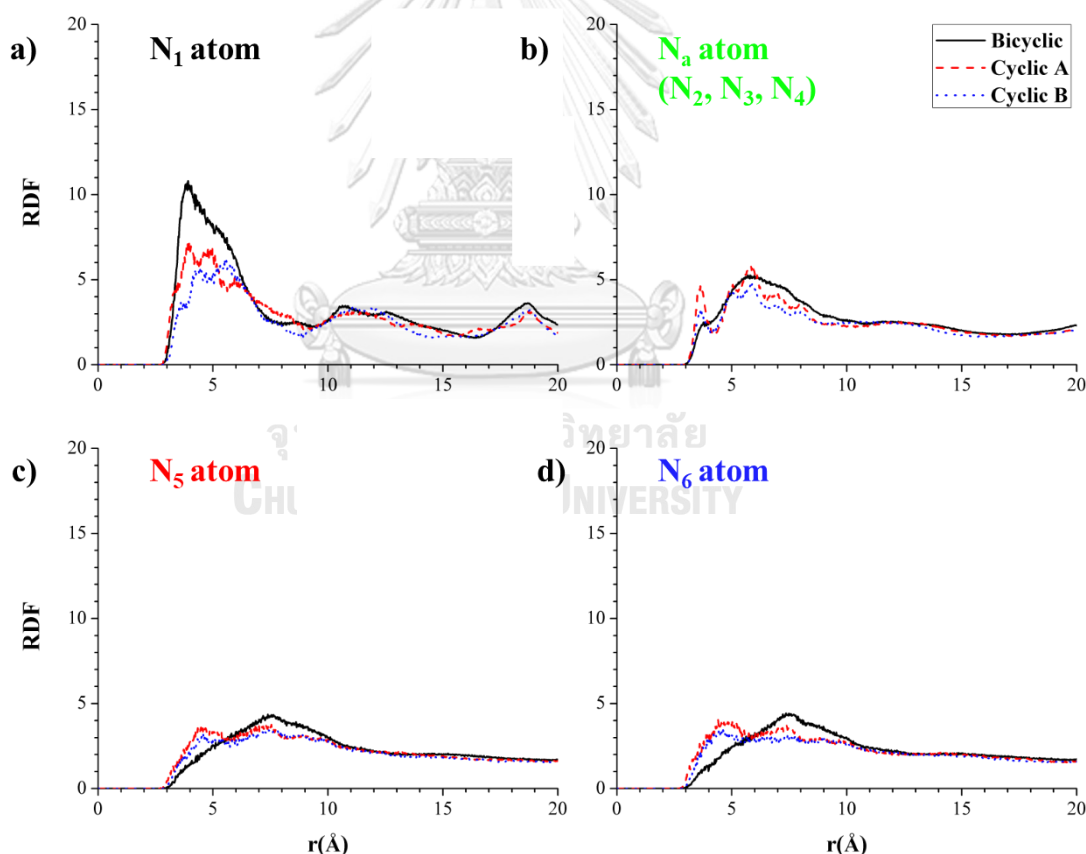


*Figure S10. Radial distribution function between structure segments of EGCG molecule and nitrogen atom in MA molecule: (a)  $N_1$ , (b)  $N_a$  (nitrogen atoms in aromatic ring:  $N_2, N_3$ , and  $N_4$ ) (c)  $N_5$ , and (d)  $N_6$ . The black-solid, red-dashed and blue dot lines represent the results obtained from bicyclic, cyclic A and cyclic B, respectively.*

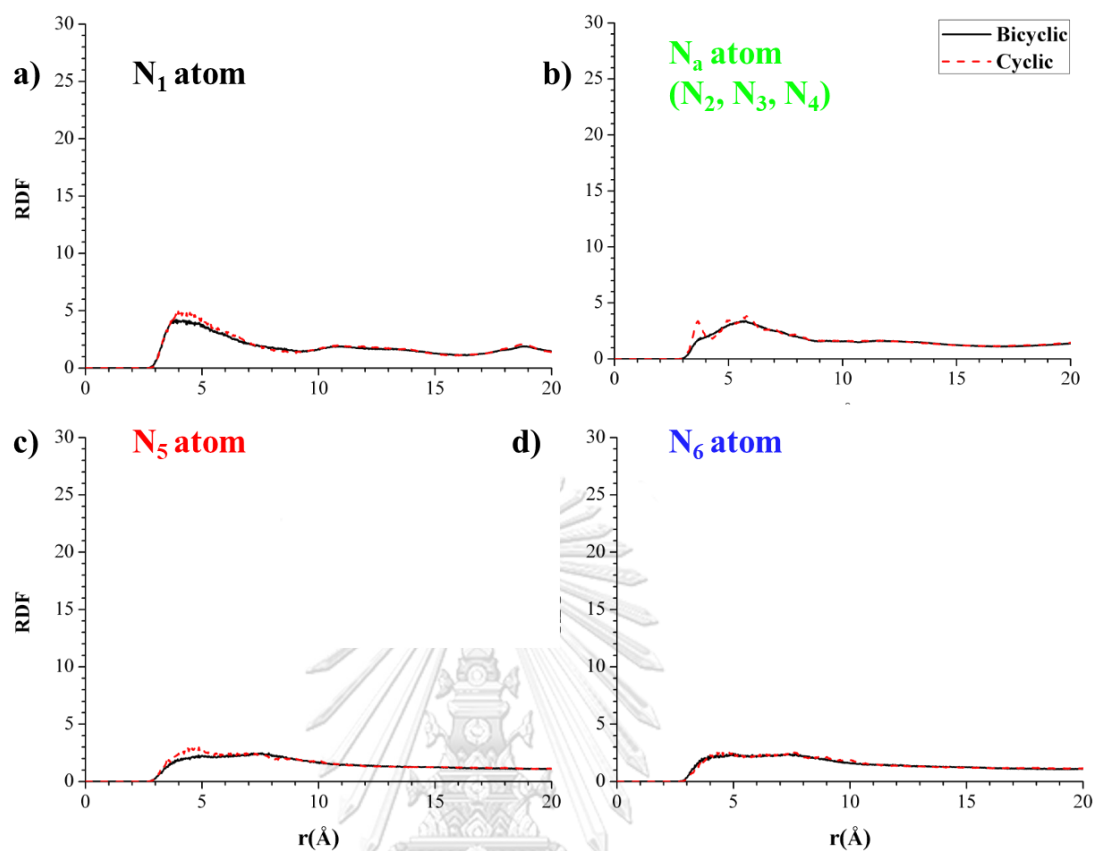


**Figure S11.** Radial distribution function between structure segments of EGC molecule and nitrogen atom in MA molecule: (a)  $N_1$ , (b)  $N_a$ , (nitrogen atoms in aromatic ring:  $N_2, N_3$ , and  $N_4$ ) (c)  $N_5$ , and (d)  $N_6$ . The black-solid, red-dashed and blue dot lines represent the results obtained from bicyclic, cyclic A and cyclic B, respectively.

## REFERENCES

1. Yashin, A., et al., *Antioxidant Activity of Spices and Their Impact on Human Health: A Review*. Antioxidants (Basel, Switzerland), 2017. **6**(3): p. 70.
2. Niemeyer, E.D. and J.S. Brodbelt, *Isomeric differentiation of green tea catechins using gas-phase hydrogen/deuterium exchange reactions*. Journal of the American Society for Mass Spectrometry, 2007. **18**(10): p. 1749-1759.
3. Esselen, M. and S.W. Barth, *Chapter Four - Food-Borne Topoisomerase Inhibitors: Risk or Benefit*, in *Advances in Molecular Toxicology*, J.C. Fishbein and J.M. Heilman, Editors. 2014, Elsevier. p. 123-171.
4. Shih, C.J., C.T. Lin, and S.M. Wu, *Adsorption of vitamin E on mesoporous titania nanocrystals*. Materials Research Bulletin, 2010. **45**(7): p. 863-869.
5. Hartmann, M., A. Vinu, and G. Chandrasekar, *Adsorption of Vitamin E on Mesoporous Carbon Molecular Sieves*. Chemistry of Materials, 2005. **17**(4): p. 829-833.
6. Liu, Y., et al., *Comparison of adsorption selectivity for (-)-epigallocatechin gallate and caffeine by porous materials modified with different amino groups*. Colloids and Surfaces A: Physicochemical and Engineering Aspects, 2017. **520**: p. 166-172.
7. Hospital, A., et al., *Molecular dynamics simulations: advances and applications*. Advances and applications in bioinformatics and chemistry : AABC, 2015. **8**: p. 37-47.
8. Hollingsworth, S.A. and R.O. Dror, *Molecular Dynamics Simulation for All*. Neuron, 2018. **99**(6): p. 1129-1143.
9. Van Der Spoel, D., et al., *GROMACS: Fast, flexible, and free*. Journal of Computational Chemistry, 2005. **26**(16): p. 1701-1718.
10. Warren, W.S., *Chapter 3 - Essential Physical Concepts for Chemistry*, in *The Physical Basis of Chemistry (Second Edition)*, W.S. Warren, Editor. 2001, Academic Press: San Diego. p. 32-59.
11. Hansen, J.-P., *Phase Transition of the Lennard-Jones System. II. High-Temperature Limit*. Physical Review A, 1970. **2**(1): p. 221-230.
12. Frenkel, D. and B. Smit, *Chapter 12 - Long-Range Interactions*, in *Understanding Molecular Simulation (Second Edition)*, D. Frenkel and B. Smit, Editors. 2002, Academic Press: San Diego. p. 291-320.
13. Cotea, V.V., et al., *Mesoporous silica SBA-15, a new adsorbent for bioactive polyphenols from red wine*. Analytica Chimica Acta, 2012. **732**: p. 180-185.

14. Yangui, A., M. Abderrabba, and A. Sayari, *Amine-modified mesoporous silica for quantitative adsorption and release of hydroxytyrosol and other phenolic compounds from olive mill wastewater*. Journal of the Taiwan Institute of Chemical Engineers, 2017. **70**: p. 111-118.
15. Karković Marković, A., et al., *Hydroxytyrosol, Tyrosol and Derivatives and Their Potential Effects on Human Health*. Molecules (Basel, Switzerland), 2019. **24**(10): p. 2001.
16. Zhao, R., et al., *Selective adsorption of tea polyphenols from aqueous solution of the mixture with caffeine on macroporous crosslinked poly(N-vinyl-2-pyrrolidinone)*. Reactive and Functional Polymers, 2008. **68**(3): p. 768-774.
17. Green, M.J., et al., *Nanotubes as polymers*. Polymer, 2009. **50**(21): p. 4979-4997.
18. Ling, X., et al., *Functionalization and dispersion of multiwalled carbon nanotubes modified with poly-L-lysine*. Colloids and Surfaces A: Physicochemical and Engineering Aspects, 2014. **443**: p. 19–26.
19. Amiri, A., et al., *One-pot, efficient functionalization of multi-walled carbon nanotubes with diamines by microwave method*. Applied Surface Science, 2011. **257**(23): p. 10261-10266.
20. Khare, K.S., F. Khabaz, and R. Khare, *Effect of Carbon Nanotube Functionalization on Mechanical and Thermal Properties of Cross-Linked Epoxy–Carbon Nanotube Nanocomposites: Role of Strengthening the Interfacial Interactions*. ACS Applied Materials & Interfaces, 2014. **6**(9): p. 6098-6110.
21. Hornak, V., et al., *Comparison of multiple Amber force fields and development of improved protein backbone parameters*. Proteins, 2006. **65**(3): p. 712-725.
22. Jakalian, A., et al., *Fast, efficient generation of high-quality atomic charges. AM1-BCC model: I. Method*. Journal of Computational Chemistry, 2000. **21**(2): p. 132-146.
23. Mark Abraham, B.H., David van der Spoel, and Erik Lindahl., *GROMACS USER MANUAL Version 5.0.4*. 2014.
24. Martin, M.G. and J.I. Siepmann, *Predicting Multicomponent Phase Equilibria and Free Energies of Transfer for Alkanes by Molecular Simulation*. Journal of the American Chemical Society, 1997. **119**(38): p. 8921-8924.
25. Showalter, S.A. and R. Brüschweiler, *Validation of Molecular Dynamics Simulations of Biomolecules Using NMR Spin Relaxation as Benchmarks: Application to the AMBER99SB Force Field*. Journal of Chemical Theory and Computation, 2007. **3**(3): p. 961-975.

26. Price, D.J. and C.L. Brooks, *A modified TIP3P water potential for simulation with Ewald summation*. The Journal of Chemical Physics, 2004. **121**(20): p. 10096-10103.
27. Liu, D., et al., *Molecular dynamics simulation of self-assembly and viscosity behavior of PAM and CTAC in salt-added solutions*. Journal of Molecular Liquids, 2018. **268**: p. 131-139.
28. Baur, J.E., *19 - Diffusion Coefficients*, in *Handbook of Electrochemistry*, C.G. Zoski, Editor. 2007, Elsevier: Amsterdam. p. 829-848.
29. Michalet, X., *Mean square displacement analysis of single-particle trajectories with localization error: Brownian motion in an isotropic medium*. Physical review. E, Statistical, nonlinear, and soft matter physics, 2010. **82**(4 Pt 1): p. 041914-041914.
30. Ziaedini, A., A. Jafari, and A. Zakeri, *Extraction of Antioxidants and Caffeine from Green Tea (Camelia sinensis) Leaves: Kinetics and Modeling*. Food Science and Technology International, 2010. **16**(6): p. 505-510.
31. McCarthy, C. and T. Vaughan, *14 - Micromechanical failure analysis of advanced composite materials*, in *Numerical Modelling of Failure in Advanced Composite Materials*, P.P. Camanho and S.R. Hallett, Editors. 2015, Woodhead Publishing. p. 379-409.
32. Ma, Y., et al., *Molecular dynamics simulation of hydrocarbon molecule adsorption on kaolinite (0 0 1) surface*. Fuel, 2019. **237**: p. 989-1002.
33. Simplício, A., J. Clancy, and J. Gilmer, *Prodrugs for Amines*. Molecules (Basel, Switzerland), 2008. **13**: p. 519-47.
34. Hall, H.K., *Correlation of the Base Strengths of Amines1*. Journal of the American Chemical Society, 1957. **79**(20): p. 5441-5444.
35. Kollman, P.A. and L.C. Allen, *Theory of the hydrogen bond*. Chemical Reviews, 1972. **72**(3): p. 283-303.
36. Quentin Kaas, M.-P.L. *IMGT/3Dstructure-DB contact analysis*. 2006 [cited 2019 November 25]; Available from: [http://www.imgt.org/IMGTEducation/Aide-memoire/\\_UK/ContactAnalysis.html](http://www.imgt.org/IMGTEducation/Aide-memoire/_UK/ContactAnalysis.html).



จุฬาลงกรณ์มหาวิทยาลัย  
**CHULALONGKORN UNIVERSITY**

## VITA

**NAME** Nutapong Tanatananon

**DATE OF BIRTH** 8 August 1994

**PLACE OF BIRTH** Bangkok

**INSTITUTIONS  
ATTENDED** 2016, B.Sc., Mahidol University

**HOME ADDRESS** 11 Moo 3, Soi Songkanong 6, Phutthamonthon Sai 6  
Road, Songkanong, Sampran, Nakhon Pathom, 73210



จุฬาลงกรณ์มหาวิทยาลัย  
CHULALONGKORN UNIVERSITY